Pesticide Biochemistry and Physiology 196 (2023) 105613

Contents lists available at ScienceDirect

Pesticide Biochemistry and Physiology

journal homepage: www.elsevier.com/locate/pest

Extraction and characterization of anti-virus anthraquinones from *Nicotiana tabacum*-derived *Aspergillus oryzae* YNCA1220

Feng-Xian Yang [a,b], Yue-Yu Ma [a], Yu-Ping Wu [c], Gao-Kun Zhao [c], Yong-Ping Li [c], Zhen-Jie Li [d], Xue-Mei Li [d], Yin-Ke Li [a,c], Wei-Guang Wang [a], Min Zhou [a], Guang-Hui Kong [c,*], Qiu-Fen Hu [a,c,*]

[a] *Key Laboratory of Chemistry in Ethnic Medicinal Resources, State Ethnic Affairs Commission & Ministry of Education, Yunnan Minzu University, Kunming 650500, PR China*
[b] *Key Laboratory of Tropical Plant Resource and Sustainable Use, Xishuangbanna Tropical Botanical Garden, Chinese Academy of Sciences, Kunming 650223, PR China*
[c] *Yunnan Academy of Tobacco Agricultural Sciences, Kunming 650031, PR China*
[d] *Yunnan Key Laboratory of Tobacco Chemistry, China Tobacco Yunnan Industrial Co., Ltd., Kunming 650031, PR China*

ARTICLE INFO

Keywords:
Aspergillus oryzae
Anthraquinones
Anti-TMV activity
Antirotavirus activity

ABSTRACT

In this study, seven novel anthraquinones (**1**–**7**) and four described anthraquinones (**8**–**11**) were purified from *Nicotiana tabacum*-derived *Aspergillus oryzae* YNCA1220. It is worth noting that only analogs of **4** and **5** have been reported as natural products to date, while the nuclei of compounds **1**–**3**, **6** and **7** were isolated for the first time in nature. Among them, compounds **1**–**3** bear an unusual anthra[2,3-*b*]furan-9,10-dione nucleus, **4** and **5** possess a rare 3-methyl-1*H*-pyrrol-2-yl substituent, and **6** and **7** are new framework anthraquinones bearing a 6-methyl-1,7-dihydro-2*H*-azepin-2-one ring. Interestingly, the in vivo assays indicated that **1**, **4** and **5** had inactivation effects against tobacco mosaic virus (TMV) with inhibition rates of 41.6%, 55.4% and 38.6%, respectively, at a concentration of 50 μg/mL, which were better than that of the positive control agent, ningnanmycin (33.8%). Compounds **1**, **4** and **5** also had protective effects with inhibition rates of 48.7%, 60.2% and 43.5% at the same concentration, while **4** had a better curative effect than ningnanmycin at a concentration of 100 μg/mL. In addition, mechanistic studies also revealed that a potent direct effect on TMV, the induction of SAR in tobacco plants, and the effective regulation of defense enzymes, defense genes, and defense hormones may be the reasons for the significant effects of **4** against TMV. At the same time, downregulation of the expression of total NtHsp70 protein by inhibiting the related *Hsp70* genes may also be involved in tobacco resistance to TMV. To evaluate whether compounds have broader antiviral activities, the antirotavirus activities of new isolates were also evaluated and found to be highly effective with a therapeutic index (TI) value ranging from 11.6 to 17.7. This study suggests that the above anthraquinone compounds, particularly **4**, have broad spectrum antiviral activities. The successful isolation and structure identification of the above anthraquinones provide new materials for the screening of anti-TMV agents and contribute to the improved utilization of *N. tabacum*-derived fungi.

1. Introduction

Endophytic fungi have been confirmed to be vital in the history of drug discovery and chemical leads with potential biological activities. As one of the most prevalent fungi in the Ascomycetes family of Trichocomaceae, *Aspergillus* is known for its ability to produce a diverse array of bioactive compounds with unique chemical structures and biological activities (Sadorn et al., 2016). Numerous endophytic *Aspergillus* species have been found to generate secondary metabolites such as alkaloids (Liang et al., 2015), butenolides (Ibrahim et al., 2015), terpenoids (Liu et al., 2019), cytochalasins (Akhter et al., 2019), phenalenones (Gombodorj et al., 2017), *p*-terphenyls (Yan et al., 2017), xanthones (Ma et al., 2015), sterols (Tawfike et al., 2019), diphenyl ether (Qin et al., 2019) and anthraquinone derivatives (Lim et al., 2012) that exhibit an extensive range of biological activities, including antifungal, antiviral, anticancer, antibacterial, antitrypanosomal, antileishmanial, and anti-inflammatory activities (Hagag et al., 2022). Among these secondary metabolites, anthraquinones (AQs), a significant class of natural and synthetic compounds, are characterized by a core skeleton of 9,10-anthracenedione (known as 9,10-

* Corresponding authors at: Yunnan Academy of Tobacco Agricultural Sciences, Kunming 650031, PR China.
E-mail addresses: yn_cigar_team@163.com (G.-H. Kong), huqf_tg@163.com (Q.-F. Hu).

https://doi.org/10.1016/j.pestbp.2023.105613
Received 17 July 2023; Accepted 6 September 2023
Available online 7 September 2023

dioxoanthracene) consisting of three fused benzene rings with two ketone groups on the central rings. AQs have diverse applications, including use as colorants (Dufossé, 2014), and have been utilized for centuries in medical applications (Masi and Evidente, 2020), such as laxatives, antimicrobial agents, and anti-inflammatory agents.

With the capacity to infect 885 plant species from 65 different families, TMV has resulted in substantial losses in contemporary agriculture (Nicaise, 2014; Song et al., 2011). There are currently limited antiviral agents available on the market to treat TMV, thus, there is a pressing demand for the development of new, efficient, and eco-friendly anti-TMV agents. In our ongoing search for anti-TMV compounds from tobacco-derived microorganisms (Yang et al., 2022a; Yang et al., 2022b), we isolated *A. oryzae* YNCA1220 from the leaves of *N. tabacum* samples. During the prefermentation work, we observed the characteristic UV absorption of anthraquinones in extracts of the strain using HPLC-UV/vis diode array detection screening. A larger fermentation led to successful isolation of seven novel (**1**–**7**) along with four known (**8**–**11**) anthraquinone derivatives (Fig. 1). Structurally, compounds **1**–**7** are rare derivatives of anthraquinone. According to our current knowledge, natural products have only reported analogs of **4** and **5** (Olaoluwa et al., 2013). The nuclei of compounds **1**–**3**, **6** and **7** were first isolated in nature. Their anti-TMV activities were evaluated, and their mechanism of disease resistance was studied in depth. Rotavirus is the main cause of dehydrated diarrhea in children under 5 years of age and requires effective treatment (Das and Bhutta, 2016; Mi et al., 2017). No specific antiviral drug has been developed for the virus. Some anthraquinones may possess similar antiviral activities against rotavirus (Sun et al., 2016). To determine whether the anthraquinones exhibit broader antiviral activities, novel isolates were also assessed for their antirotavirus properties. This study reports the purification, determination, and antiviral assessment of new isolates.

2. Materials and methods

2.1. General experimental procedures for the isolation and identification of compounds

NMR spectra were acquired using a DRX-500 NMR spectrometer (Bruker, Billerica, USA), with TMS serving as the internal standard. IR measurements were conducted using a Nicolet iS10 FT-IR spectrometer (Thermo Fisher Scientific, USA), while UV spectra were acquired in MeOH using a Shimadzu UV-1900 spectrophotometer (Shimadzu, Kyoto, Japan). HRESIMS spectra were taken on a Shimadzu UPLC-IT-TOF mass spectrometer. Silica gel (200–300 mesh, Qing-dao Marine Chemical, Inc. located in Qingdao, China), Sephadex LH-20 (supplied by Sigma-Aldrich, Inc. based in USA) and Lichroprep RP-18 gel (40–63 μm, Merck, Darmstadt, Germany) were utilized for column chromatography (CC). Preparative HPLC was conducted on an Agilent 1260 HPLC system equipped with a photodiode array detector using a Zorbax PrepHT GF C_{18} 21.2 mm × 25 cm column. Isocratic elution conditions and 12 mL/min flow rate were employed at room temperature. To monitor column fractions, thin-layer chromatography (TLC) was employed, and visualization was accomplished using two methods. The first method involved UV absorption at 254 and 365 nm, while the second method involved spraying the plates with a mixture of 5% H_2SO_4 in ethanol and subsequently heating them.

2.2. Biological material

The fungal strain was isolated from the leaf of *N. tabacum*, which is commonly known as cigar tobacco. The leaf was acquired from Gengma County, located in Lincang Prefecture of Yunnan Province, in 2020 and identified as *A. oryzae* YNCA1220 (GenBank accession no. KM999950). The identification of the fungus was performed by sequencing the ITS region followed by a BLAST search in NCBI. After confirmation, the strain was deposited in China Tobacco Yunnan Industrial Co., Ltd. in Kunming.

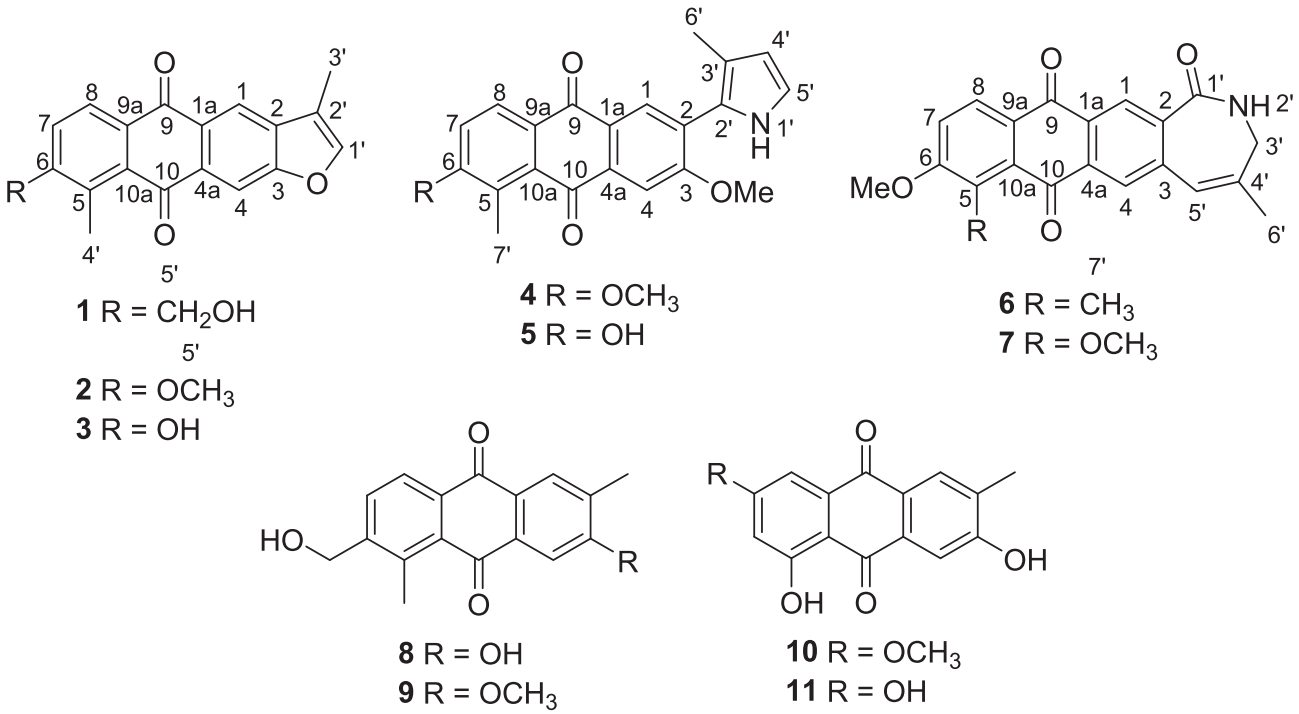

Fig. 1. Structures of compounds **1**–**11**.

2.3. Fermentation of A. oryzae YNCA1220

To generate spores, strain YNCA1220 was cultivated on potato dextrose agar (PDA) plates. Next, agar plugs were inoculated into a 250 mL Erlenmeyer flask containing 50 mL of seed medium composed of potato dextrose broth (pH not adjusted) and incubated for 5 days at 30 °C on a rotary shaker (200 rpm). Subsequently, a 10 mL sample of the seed culture was transferred into a 500 mL Fernbach flask that contained 200 g of rice and 240 mL of distilled water. The flask was then incubated at 25 °C for a period of 45 days. This study utilized a total of 100 Erlenmeyer flasks.

2.4. Extraction and purification

The fermentation broth was extracted using 70% aq. Me_2CO (4 × 20 L), filtered and concentrated under reduced pressure until Me_2CO was free. The resulting extract was then subjected to extractions with EtOAc three times, resulting in an EtOAc extract (80.6 g). The crude extract was then subjected to CC (SiO_2) by eluting stepwise using a $CHCl_3$/MeOH gradient system (20:1, 8:2, 7:3, 6:4, 5:5, *v*/v), which resulted in seven fractions A–G. Fr·C (20.0 g) was further subjected to silica gel CC with $CHCl_3$/Me_2CO (9:1, 8:2, 7:3, 6:4, 5:5, v/v) as the mobile phase, affording eight subfractions (Fr·C1–Fr·C8). After obtaining subfraction Fr·C2 (160.0 mg), further purification was carried out using preparative HPLC. Isocratic elution was performed using a mixture of MeOH/H_2O (65%, *v*/v), which resulted in the formation of **6** (20.0 mg) and **7** (15.0 mg). Fr·C3 (5.0 g) was subjected to CC (Sephadex LH-20) by eluting using $CHCl_3$/MeOH to obtain subfractions Fr·C3–1–Fr·C3–10. Compounds **4** (16.5 mg) and **5** (14.6 mg) were obtained through the isolation process of Fr·C3–4 (450.0 mg), which was purified by preparative HPLC using MeOH/H_2O isocratic elution (60%, *v*/v). Using a gradient with decreasing solvent polarity, Fr·D (8:2, 10.5 g) underwent RP-18 CC and yielded eight subfractions (Fr·D1–Fr·D8) by utilizing mixtures of MeOH/H_2O (20%, 40%, 60%, 80%, v/v). Fr·D4, which weighed 540.0 mg, underwent additional separation on Sephadex LH-20 CC using MeOH as the mobile phase. This process resulted in the formation of Fr·D4–9, which weighed 110.0 mg, and preparative HPLC purification of Fr·D4–9 using MeCN/H_2O (35%, v/v) yielded compounds **1** (15.0 mg), **2** (17.5 mg) and **3** (9.5 mg). Fr·E (7:3, 16.0 g) was subjected to RP-18 CC and eluted with MeOH/H_2O (20%, 40%, 60%, 80%, v/v), and preparative HPLC afforded compounds **8** (20.0 mg) and **9** (10.5 mg) (using MeOH/H_2O 55%, v/v as the mobile phase) together with **10** (15.3 mg) and **11** (12.0 mg) (using MeOH/H_2O 36%, v/v as the mobile phase).

6-Hydroxymethyl-2′,5-dimethylanthra [2,3-*b*] furan-9,10-dione (1) purified as a reddish gum; UV (MeOH) λ_{max} (log ε) 215 (4.32), 264 (3.52), 286 (3.60), 410 (3.46) nm; IR (KBr) ν_{max} 3396, 3042, 2960, 2812, 1668, 1615, 1576, 1438, 1342, 1160, 1024, 862 cm^{-1}; Table 1 provides ^1H and ^{13}C NMR data; HRESIMS *m/z* 329.0787 $[M + Na]^+$ (calcd for $C_{19}H_{14}NaO_4$, 329.0790).

6-Methoxy-2′,5-dimethylanthra [2,3-*b*] furan-9,10-dione (2) purified as a reddish gum; UV (MeOH) λ_{max} (log ε) 215 (4.36), 266 (3.58), 289 (3.64), 412 (3.38) nm; IR (KBr) ν_{max} 3062, 2968, 2834, 1666, 1616, 1552, 1443, 1326, 1148, 1057, 768 cm^{-1}; Table 1 provides ^1H and ^{13}C NMR data; HRESIMS *m/z* 329.0796 $[M + Na]^+$ (calcd for $C_{19}H_{14}NaO_4$, 329.0790).

6-Hydroxyl-2′,5-dimethylanthra [2,3-*b*] furan-9,10-dione (3) purified as a reddish gum; UV (MeOH) λ_{max} (log ε) 215 (4.36), 266 (3.58), 289 (3.64), 412 (3.38) nm; IR (KBr) ν_{max} 3415, 3057, 2964, 2830, 1668, 1612, 1557, 1445, 1332, 1125, 1060, 804 cm^{-1}; Table 1 provides ^1H and ^{13}C NMR data; HRESIMS *m/z* 315.0627 $[M + Na]^+$ (calcd for $C_{18}H_{12}NaO_4$, 315.0633).

3,6-Dimethoxy-5-methyl-2-(3′-methyl-1′*H*-pyrrol-2′-yl)anthracene-9,10-dione (4) purified as a reddish gum; UV (MeOH) λ_{max} (log ε) 212 (4.46), 260 (3.61), 284 (3.58), 408 (3.42) nm; IR (KBr) ν_{max} 3358, 3126, 3057, 2938, 2842, 1665, 1618, 1524, 1439, 1342, 1135, 1064, 769 cm^{-1}; Table 2 provides ^1H and ^{13}C NMR data; HRESIMS *m/z* 384.1217 $[M + Na]^+$ (calcd for $C_{22}H_{19}NNaO_4$, 384.1212).

6-Hydroxy-3-methoxy-5-methyl-2-(3′-methyl-1′*H*-pyrrol-2′-yl) anthracene-9,10-dione (5) purified as a reddish gum; UV (MeOH) λ_{max} (log ε) 212 (4.42), 258 (3.64), 283 (3.62), 406 (3.45) nm; IR (KBr) ν_{max} 3416, 3354, 3132, 3055, 2940, 2846, 1668, 1614, 1532, 1435, 1348, 1139, 1060, 773 cm^{-1}; Table 2 provides ^1H and ^{13}C NMR data; HRESIMS *m/z* 370.1050 $[M + Na]^+$ (calcd for $C_{21}H_{17}NNaO_4$, 370.1055).

6-Methoxy-4′,5-dimethyl-2′,3′-dihydro-1′*H*-anthra [2,3-*c*] azepine-1′,9,10-trione (6) purified as a reddish gum; UV (MeOH) λ_{max} (log ε) 215 (4.36), 268 (3.68), 415 (3.58) nm; IR (KBr) ν_{max} 3342, 3138, 2946, 1668, 1655, 1620, 1542, 1463, 1348, 1274, 1162, 1059, 842 cm^{-1}; Table 3 provides ^1H and ^{13}C NMR data; HRESIMS *m/z* 370.1064 $[M + Na]^+$ (calcd for $C_{21}H_{17}NNaO_4$, 370.1055).

5,6-Dimethoxy-4′-methyl-2′,3′-dihydro-1′*H*-anthra [2,3-*c*] azepine-1′,9,10-trione (7) purified as a reddish gum; UV (MeOH) λ_{max} (log ε) 215 (4.32), 271 (3.73), 418 (3.64) nm; IR (KBr) ν_{max} 3348, 3135, 2960, 1670, 1656, 1617, 1554, 1468, 1342, 1265, 1169, 1054, 829 cm^{-1}; Table 3 provides ^1H and ^{13}C NMR data; HRESIMS *m/z* 386.3597 $[M + Na]^+$ (calcd for $C_{21}H_{17}NNaO_5$, 386.3588).

Table 1
^1H and ^{13}C NMR data of compounds **1**–**3** (data acquired in $CDCl_3$, 500 MHz, δ in ppm).

No.	**1**		**2**		**3**	
	δ_C, type	δ_H, mult (*J* in Hz)	δ_C, type	δ_H, mult (*J* in Hz)	δ_C, type	δ_H, mult (*J* in Hz)
1	123.5, CH	8.11 s	123.2, CH	8.12 s	123.3, CH	8.10 s
1a	132.8, C		132.0, C		132.4, C	
2	130.3, C		134.1, C		133.9, C	
3	159.5, C		158.2, C		158.0, C	
4	112.6, CH	7.94 s	116.6, CH	7.96 s	116.4, CH	7.95 s
4a	136.7, C		135.8, C		135.6, C	
5	138.2, C		124.3, C		125.9, C	
6	143.6, C		161.8, C		158.9, C	
7	131.1, CH	7.51 d (7.8)	118.9, CH	6.93 d (7.8)	120.0, CH	6.88 d (7.8)
8	128.7, CH	7.72 d (7.8)	128.2, CH	7.64 d (7.8)	129.0, CH	7.61 d (7.8)
9	181.0, C		181.2, C		181.2, C	
9a	133.9, C		126.8, C		127.2, C	
10	179.9, C		180.0, C		180.0, C	
10a	135.6, C		136.9, C		137.2, C	
1′	140.2, CH	7.40 s	140.5, CH	7.41 s	140.7, CH	7.40 s
2′	118.4, C		118.2, C		118.3, C	
3′	10.5, CH_3	2.04 s	10.8, CH_3	1.99 s	10.9, CH_3	2.0 s
4′	11.9, CH_3	2.30 s	8.9, CH_3	2.17 s	8.0, CH_3	2.14 s
5′	63.3, CH_2	4.60 s	56.2, CH_3	3.82 s		
Ar-OH						10.85 s

Table 2
^{1}H and ^{13}C NMR data of compounds **4** and **5** (data acquired in $CDCl_3$, 500 MHz, δ in ppm).

No.	**4**		**5**	
	δ_C, type	δ_H, mult (*J* in Hz)	δ_C, type	δ_H, mult (*J* in Hz)
1	131.8, CH	7.97 s	131.8, CH	7.95 s
1a	128.9, C		128.6, C	
2	124.9, C		124.7, C	
3	158.5, C		158.3, C	
4	115.3, CH	7.37 s	115.4, CH	7.35 s
4a	132.5, C		132.7, C	
5	125.9, C		126.3, C	
6	162.1, C		158.7, C	
7	118.2, CH	6.95 d (7.8)	120.1, CH	6.91 d (7.8)
8	127.0, CH	7.76 d (7.8)	128.1, CH	7.73 d (7.8)
9	180.9, C		181.0, C	
9a	125.4, C		127.0, C	
10	179.8, C		179.9, C	
10a	135.9, C		136.9, C	
1′		7.61 s		7.61 s
2′	130.5, C		130.7, C	
3′	116.9, C		116.9, C	
4′	109.4, CH	6.19 d (2.8)	109.5, CH	6.18 d (2.8)
5′	116.1, CH	6.73 d (2.8)	116.1, CH	6.73 d (2.8)
6′	11.3, CH_3	1.89 s	11.3, CH_3	1.88 s
7′	8.6, CH_3	2.13 s	8.24, CH_3	2.02 s
3-OMe	56.0, CH_3	3.80 s	56.0, CH_3	3.79 s
6-OMe	56.2, CH_3	3.84 s		
Ar-OH				10.85, s

Table 3
^{1}H and ^{13}C NMR data of compounds **6** and **7** (data acquired in $CDCl_3$, 500 MHz, δ in ppm).

No.	**6**		**7**	
	δ_C, type	δ_H, mult (*J* in Hz)	δ_C, type	δ_H, mult (*J* in Hz)
1	127.8, CH	8.50, s	127.6, CH	8.47, s
1a	131.7, C		131.0, C	
2	132.2, C		132.5, C	
3	140.1, C		139.8, C	
4	125.5, CH	8.10, s	125.7, CH	8.11, s
4a	138.3, C		138.4, C	
5	124.6, C		150.7, C	
6	161.6, C		154.3, C	
7	118.3, CH	6.92, d (7.8)	119.2, CH	6.96, d (7.8)
8	128.3, CH	7.66, d (7.8)	124.6, CH	7.43, d (7.8)
9	181.3, C		181.5, C	
9a	126.3, C		129.6, C	
10	180.1, C		180.3, C	
10a	136.5, C		120.9, C	
1′	165.3, C		165.6, C	
2′		5.44, t (5.4)		5.45, t (5.4)
3′	58.2, CH_2	4.52, d (5.4)	58.5, CH_2	4.50, d (5.4)
4′	133.9, C		133.6, C	
5′	131.2, CH	6.44, s	131.6, CH	6.44, s
6′	19.8, CH_3	1.86, s	19.7, CH_3	1.87, s
7′	8.7, CH_3	1.98, s		
5-OMe			61.2, CH_3	3.85, s
6-OMe	56.2, CH_3	3.82, s	56.4, CH_3	3.82, s

2.5. Anti-TMV activity assays

To conduct the tests, TMV was first purified through the Gooding method and then diluted with 0.01 M phosphate-buffered saline (PBS) to achieve a 50 μg/mL concentration (Gooding Jr. and Hebert, 1967). This TMV solution was then used in the study. The tests were carried out on plants at the five- to six-leaf stage. *Nicotiana glutinosa* was used for in vivo inactivation and protection activities against TMV, while *N. tabacum* cv. HD, which is a commonly grown tobacco variety (China), was used for curative activities against TMV and systemic TMV infection. To determine the inactivation and protection activities against TMV, the tested compounds were dissolved in DMSO and diluted with distilled water to a concentration of 50 μg/mL, while the tested compounds had curative activities against TMV at a concentration of 100 μg/mL. The solution (the same volume of DMSO and H_2O) was employed as a negative control (CK), while the new cytosine nucleoside peptide antiviral agent ningnanmycin ($C_{16}H_{25}N_7O_8$, CAS#: 156410–09-2) was used as a positive control. Each isolate and control agent was repeated three times.

2.5.1. Investigation of inactivation activities against TMV

To determine the inactivation activities against TMV, the half-leaf method was used as mentioned earlier (Hu et al., 2013; Zhou et al., 2015). Briefly, the tested compound solutions were mixed with TMV in equal volumes. Subsequently, the mixture was inoculated onto the left side of the *N. glutinosa* leaves after 30 min, while a mixture of solvent and virus was inoculated onto the right side as a control. The numbers of local lesions were documented 3–4 days post inoculation, and the rates of inhibition were computed:

$$\text{inhibition rate } (\%) = [(C - T)/C] \times 100\% \quad (1)$$

Here, C represents the mean number of local lesions observed in the control, while T represents the mean number of lesions observed in the treatment.

To determine the IC_{50} values for inactivation effects, a dose-response assay was conducted. The assay involved testing a variety of concentrations (200, 100, 50, 25, 12.5, 6.25, 3.125 μg/mL) of both the compound under study and a positive control agent against TMV. The anti-TMV activities were measured with each concentration of the samples. Using GraphPad Prism, the IC_{50} values were calculated by fitting the data to a dose-response curve using a nonlinear regression model. The concentration of the sample required to inhibit 50% of TMV activity was then determined as the IC_{50} value.

2.5.2. Investigation of protection activities against TMV

The compounds, ningnanmycin, a same volume of DMSO and H_2O solution were smeared on the whole tobacco leaves (at least 5 leaves). After 6 h, 100 μL TMV (50 μg/mL) was inoculated on the whole leaf. Each inoculated leaf was washed with water after 30 min. The number of local lesions was recorded 3–4 days after inoculation. The inhibition rate was calculated by formula I.

2.5.3. Investigation of curative activities against TMV

In China, flue-cured tobacco is the most widely cultivated tobacco, accounting for more than 95% of the tobacco planting area. To better apply the laboratory results to the actual planting process, we selected flue-cured tobacco (*N. tabacum* cv. HD, China's main flue-cured tobacco cultivar) for curative activity experiments. Tobacco seedlings at the 5–6 leaf stage that had been infected with TMV were selected, and the growth and the degree of infection were basically the same. The leaves were evenly brushed with 100 μg/mL samples using a fine brush, brushed again after 10 days, and observed after 20 days. The curative effect was recorded by taking photos.

2.5.4. Determination of the direct effect of compound **4** on TMV

Morphological observation of TMV particles via transmission electron microscopy (TEM, FEI TECNAI BIO, USA) was used to detect the direct effect of **4** on TMV. A mixture of TMV (25 μg/mL) and a solution of compound **4** (250 μg/mL) of equal volumes was prepared at 25 °C for 60 min. Subsequently, the mixture was placed on carbon-coated grids and stained negatively with 0.01 mL of 2% phosphotungstic acid for 1 min. As a control, a solution of 1% DMSO solution mixed with TMV solution (25 μg/mL) at the same volume was used. The impact of compound **4** on TMV was directly observed by examining morphological changes in TMV particles (Li et al., 2021).

2.5.5. Effects of compounds on systemic infection of TMV

The experiment in this part was carried out according to the reported

methods (Yan et al., 2022). Healthy *N. tabacum* cv. HD plants were used for the purpose of this study. The entire plant was smeared with a compound solution of 50 μg/mL, while a negative control of the solvent and a positive control of ningnanmycin were also used. After 12 h in a greenhouse without insects, the 3rd to 4th leaves from the top were infected using TMV. Three treatments were set up: solvent + TMV (CK^{-}), ningnanmycin + TMV (N), and compounds + TMV. The leaves were collected on the 3rd and 7th days after inoculation, TMV-CP was then detected by western blot assay, and *TMV-CP*, *NtHsp70–1*, *NtHsp70–261*, *NbHsp70cp-1*, *NbHsp70c–A*, *PR-1* and *PR-5* were detected by PCR.

2.5.5.1. SDS-PAGE and western blot analysis of TMV-CP and Hsp70. Anti-β-Actin mouse monoclonal antibody (Plant) (CW0264M), primary antibody against TMV-CP (SRA57400/10), and primary antibody against heat shock protein 70 (AS09 592) were purchased from Beijing Com Win Biotech Co., Ltd., American Agdia Corporation, and Swedish Agrisera Corporation, respectively. The remaining reagents used in the SDS-PAGE and western blot experiments were purchased from Solarbio Science & Technology Co., Ltd., Beijing, China. Protein loading buffer (containing 10 mL/L β-ME, 40 g/L SDS, 2 g/L bromophenol blue, 200 mL/L glycerin, and 0.1 mol/L Tris-HCl, pH 6.8) was utilized to grind the leaves (0.1 *g*), and then centrifuged before the supernatants were taken for quantification. Protein extract (dissolved in 5 × sample loading buffer) was boiled for 7 min and subjected to SDS-PAGE before being transferred to PVDF membranes (Millipore, St. Louis, USA). The membranes were blocked using 5% nonfat milk and incubated overnight with primary antibodies (anti-TMV, anti-Hsp70, and anti-β-actin) at 4 °C and then incubated with fluorescently labeled secondary antibodies (anti-rabbit IgG) conjugated to horseradish peroxidase for 1 h at room temperature. The membranes were then incubated with Pierce ECL substrate (Thermo Scientific), and proteins of interest were visualized using chemiluminescent detection on an Image Quant LAS 4000 mini (GE Healthcare) (Yan et al., 2018). The density of bands was quantified by using ImageJ software (NIH, Bethesda, MD, United States) and normalized to the actin density for calculating total protein.

2.5.5.2. RT-PCR analysis of TMV-CP and quantitative real-time PCR analysis of Hsp70 genes and defense-related genes. A FastPure Universal Plant Total RNA Isolation kit (Vazyme Biotech Co., Ltd.) was utilized to extract total RNA from 0.1 g fresh tobacco leaves, in accordance with the instructions provided by the manufacturer. Following the manufacturer's instructions, the RNA was purified and subjected to reverse transcription with HiScript III RT SuperMix for qPCR (+gDNA wiper) (Vazyme Biotech Co., Ltd.). RT-PCR was conducted using 2 × Taq Master Mix (Dye Plus) purchased from Vazyme Biotech Co., Ltd., for *TMV-CP*. The genes of interest were visualized using Azure Biosystems C150 (Azure Biosystems, United States). The density of bands was quantified by using ImageJ software and normalized to the NtRbcs density for calculating gene expression. qRT-PCR was conducted using ChamQ Universal SYBR qPCR Master Mix purchased from Vazyme Biotech Co., Ltd. for *NtHsp70–1*, *NtHsp70–261*, *NbHsp70cp-1*, *NbHsp70c-A*, *PR-1* and *PR-5* on a LightCycle 480 II (Roche, Germany). Table S1 includes the primer sequences.

2.5.6. Defense enzyme activities assay

The pretreatment methods used in this part for plants and samples were the same as those in 2.5.5. Leaf samples were collected at different intervals (1, 3, 5, and 7 days after spraying) and ground up. Adding 1 mL of protein extraction solution from the kit to 0.1 g of homogenate, the mixture was subjected to ultrasonic waves for 10 min. Subsequently, the solution was centrifuged at 8000 rpm (8500 *g*) for 5 min, and the resulting supernatant was preserved (Hu et al., 2022; Jiang et al., 2022; Yan et al., 2022). The effects of compounds on the activities of superoxide dismutase (SOD, EC number: 1.15.1.1), peroxidase (POD, EC number: 1.11.1.1), polyphenol oxidase (PPO, EC number: 1.10.3.1), and phenylalanine ammonia lyase (PAL, EC number: 4.3.1.24) in *N. tabacum* cv. HD plants were investigated using kits from Shanghai Tongwei Biotechnology Co., Ltd., China. Healthy tobacco was denoted as mock. Each treatment included three tobacco plants.

2.5.7. Investigation of SA and MDA content

The pretreatment methods of plants and samples as well as the sampling time were the same as those described in 2.5.5. and 2.5.6. (Hu et al., 2022; Jiang et al., 2022; Yan et al., 2022). Salicylic acid (SA) and malondialdehyde (MDA) contents were measured by SA and MDA assay kits according to the manufacturer's instructions (Shanghai Tongwei Biotechnology Co., Ltd., China). Healthy tobacco was denoted as mock. Each treatment included three tobacco plants.

2.5.8. Molecular docking

The present study utilized AutoDock Vina software to perform molecular docking calculations (Malla et al., 2023; Sachse et al., 2007; Xiao et al., 2015). The protein sequence was obtained from the NCBI database, and the 3D crystal protein structure was obtained from RCSB PDB database (PDB:2OM3). The ligand structures were generated using chem3D. To prepare for molecular docking calculations, the pdbqt files for the proteins and ligands were created based on the AutoDock protocol, with all docking parameters set to their default values, except for the maximum number of energy evaluations (eval) and the number of genetic algorithm (GA) runs. A docking grid was created for the receptor binding site, with a grid size of 40 Å * 40 Å * 40 Å and a grid spacing value of 0.375 Å. Gasteiger atomic partial charges were assigned to all ligands under investigation.

2.6. Antirotavirus activity assay

To assess the antirotavirus efficacy, an in vitro MA104 cell culture was infected with the human rotavirus Wa group (obtained from the Institute of Medical Biology, Chinese Academy of Medical Sciences in Kunming, China). The objective of the study was to determine the half maximal effective concentration (EC_{50}) and half cytotoxicity concentration (CC_{50}) of the tested compounds, with ribavirin (Hubei Hanwei Chemical Co., Wuhan, China) serving as a positive control, as outlined in the literature (Hu et al., 2021). To conduct the experiment, a density of 1×10^5 cells per well was used to culture MA-104 cells in 96-well plates for a duration of 48 h. Subsequently, fresh media containing varying concentrations of the compounds being tested were added to the wells, and the cells were incubated for 72 h. After this, the media were removed, MTT solution was introduced, and the plates were then incubated at 37 °C for a duration of 4 h. Subsequently, 100 μL of a solution containing 0.04 mol/L HCl and isopropanol was added to facilitate the dissolution of the formazan crystals. The measurement of absorbance at 540 nm using a microplate reader (SpectraMax190, Microg Biotech, Guangzhou, China) was subsequently carried out, wherein the background absorbance at 655 nm was subtracted before the actual measurement. Regression analysis was used to estimate the 50% CC_{50} of each compound.

During the mixed treatment test, the rotaviruses and compounds were mixed at a multiplicity of infection (MOI) of 0.01 with varying concentrations of the compounds ranging from 1 to 160 μg/mL. The mixture was then allowed to incubate at a temperature of 4 °C for an hour. Following the incubation period, the mixture was applied to near confluent MA-104 cell monolayers (with 1×10^5 cells per well) in triplicate and shaken occasionally for an hour. Following this, the mixed solution was eliminated, and the cells were washed with Eagle's minimum essential medium (EMEM) before being exposed to EMEM supplemented with 1.0 μg/mL trypsin. The cells were subsequently placed inside an incubator and incubated for 72 h at 37 °C under a 5% CO_2 atmosphere until the viral cytopathic effect (CPE) was detected in the control cells via light microscopy. Regression analysis was employed to

estimate the EC_{50}.

2.7. Statistical analysis

A fully randomized design was utilized for each measurement, which was repeated three times. Statistical analyses were conducted using GraphPad Prism 7.0 and Microsoft Excel 2016. Data were analyzed by analysis of variance using Duncan's multiple range tests and *t*-tests in GraphPad Prism 7.0 and by calculating the least significant difference (LSD) at a significance of 0.05 using different letters. The tables were furnished with a value representing the standard deviation (± SD), while the column was adorned with an error bar. If the relative expression values were higher than one, it meant that there was an elevation in gene accumulation in tobacco tissues compared to mock inoculated, whereas values lower than one suggested a decrease in expression levels.

3. Results and discussion

3.1. Purification and structure determination of compounds

By subjecting the EtOAc extract of *A. oryzae* YNCA1220 to CC together with preparative HPLC multiple times, seven undescribed anthraquinones (**1**–**7**) and four described analogs (**8**–**11**) were obtained. The structures of these isolates, along with their ^{1}H and ^{13}C NMR information, are displayed in Fig. 1 and Tables 1–3, respectively. The described isolates were identified as 3-hydroxy-6-hydroxymethyl-2,5-dimethylanthraquinone (**8**), 6-hydroxymethyl-3-methoxy-2,5-dimethylanthraquinone (**9**) (Wu et al., 2021), macrosporin (**10**) (Ge et al., 2005) and 1,3,7-trihydroxy-6-methylanthraquinone (**11**) (Hosoe et al., 1990) by comparison with previously reported data.

One of the new isolates, compound **1**, was acquired as a reddish gum. The HRESIMS data suggested its molecular formula to be $C_{19}H_{14}O_4$, indicating 13 indices of hydrogen deficiency. The ^{1}H NMR spectrum of **1** exhibited resonances indicative of a set of *ortho*-coupled aromatic protons at 7.51 (d, 7.8 Hz, H-7) and 7.72 (d, 7.8 Hz, H-8), three aromatic singlet protons at δ_H 8.11 (s, H-1), 7.94 (s, H-4), and 7.40 (s, H-1′), a hydroxymethyl group at δ_H 4.60 (s, H_2-5′), and two methyl groups at δ_H 2.04 (s, H_3-3′) and 2.30 (s, H_3-4′). Analysis of the molecular formula, ^{13}C NMR, DEPT and HSQC spectra led to the presence of 19 carbons, containing two carbonyls at δ_C 181.0 (C-9) and 179.9 (C-10), five aromatic methine carbons, nine aromatic quaternary carbons, and three aliphatic carbon signals (two methyl carbons and one hydroxymethyl carbon). Further HMBC correlations between H-1 and C-4a/C-3/C-9/C-2′, H-4 and C-1a/C-10/C-2, H-7 and C-5/C-9a, H-8 and C-6/C-10a/C-9, and H-1′ and C-2/C-3 suggested the presence of anthra[2,3-*b*]furan-5,10-dione nuclei, similar to those of known compounds (Fig. 2) (Tikhomirov et al., 2014). In addition, HMBC correlations between H-3′ and C-1′/C-2′/C-2, H-4′ and C-5/C-6/C-10a, and H-5′ and C-5/C-6/C-7 demonstrated that two methyls and one hydroxymethyl were located at C-2′, C-5 and C-6, respectively (Fig. 2). Based on these findings, the structure of **1** was determined to be 6-hydroxymethyl-2′,5-dimethylanthra[2,3-*b*]furan-9,10-dione (Fig. 1).

The characteristic UV spectra of **2** (412, 289, 266 nm) and **3** (412, 289, 266 nm) were similar to those of **1**, suggesting that **2** and **3** were anthra[2,3-*b*]furan-9,10-dione analogs. Both of them were isolated as a reddish gum. The molecular formula of **2** was deduced as $C_{19}H_{14}O_4$, which was the same as that of **1**. The analysis of 1D and 2D NMR spectra indicated a notable difference, with the signals for the hydroxymethyl group at C-6 being observed as a methoxy group (δ_H 3.82; δ_C 56.2) in compound **2** (Table 1). Thus, compound **2** was assigned and named 6-methoxy-2′,5-dimethylanthra[2,3-*b*]furan-9,10-dione. The HRESIMS of **3** supported its molecular formula of $C_{18}H_{12}O_4$, indicating 13 indices of hydrogen deficiency. A molecular mass 14 Da less than that of **2** was established for **3**. Both compounds exhibited comparable NMR spectra, with the exception of lacking a methoxy signal in **2** and exhibiting a phenolic hydroxyl signal (δ_H 10.85) in **3**, named 6-hydroxyl-2′,5-dimethylanthra[2,3-*b*]furan-9,10-dione.

Compound **4**, a reddish gum, had a molecular formula of $C_{22}H_{19}NO_4$ with 14 indices of hydrogen deficiency, which was confirmed from its HRESIMS as well as its ^{13}C NMR data. It is an anthraquinone derivative because its UV spectrum was similar to those of **1**, **2** and **3**. The ^{1}H NMR spectrum (Table 2) contained resonances associated with six aromatic protons δ_H 7.97 (s, H-1), 7.37 (s, H-4), 6.95 (d, 7.8 Hz, H-7), 7.76 (d, 7.8 Hz, H-8), 6.19 (d, 2.8 Hz, H-4′) and 6.73 (d, 2.8 Hz, H-5′), two methyl protons δ_H 1.89 (s, H_3-6′) and 2.13 (s, H_3-7′), two methoxy protons δ_H 3.80 (s, 3-OCH_3) and 3.84 (s, 6-OCH_3), and an active proton δ_H 7.61 (s, NH). Based on the ^{13}C NMR, DEPT and HSQC spectra, it was determined that there are 22 carbons, containing two carbonyls, ten aromatic quaternary carbons, six aromatic methine carbons, two methoxy carbons and two methyl carbons. HMBC correlations between H-1 and C-4a/C-3/C-9, H-4 and C-1a/C-2/C-10, H-7 and C-5/C-9a, and H-8 and C-10a/C-6/C-9 (Fig. 2) suggested the presence of a 2,3,5,6-tetrasubstituted-9,10-anthraquinone skeleton. Further HMBC correlations between H-4′ and C-2′, H-5′ and C-2′/C-3′, H_3-6′ and C-2′/C-3′/C-4′, H-NH and C-3′/C-4′ and the remaining three indices of hydrogen deficiency established a 3′-methyl-1′*H*-pyrrole which located at C-2 from the HMBC correlations of H-NH with C-2 and H-1 with C-2′ (Fig. 2). The remaining substituent positions were determined by the HMBC correlations between H_3-3-OCH_3 and C-3, H_3-6-OCH_3 and C-6 and H_3-7′ and C-5. Therefore, compound **4** was assigned as 3,6-dimethoxy-5-methyl-2-(3′-methyl-1′*H*-pyrrol-2′-yl)anthracene-9,10-dione.

Compound **5** was purified as a reddish gum. Its molecular formula was deduced to be $C_{21}H_{17}NO_4$, which was a molecular mass 14 Da less than that of **4**. Its UV spectrum resembled that of **4**. A comparison of the NMR data between **4** and **5** revealed that the methoxy group at C-6 in **4** was substituted by a hydroxyl group in **5**. The ^{1}H NMR data exhibited a phenolic hydroxyl proton δ_H 10.85 (s). Ultimately, compound **5** was clarified as 6-hydroxy-3-methoxy-5-methyl-2-(3′-methyl-1′*H*-pyrrol-2′-yl)anthracene-9,10-dione.

Compound **6** was purified as a reddish gum, and its molecular formula was established as $C_{21}H_{17}NO_4$, implying 14 indices of hydrogen deficiency. A thorough analysis of the ^{1}H NMR, ^{13}C NMR, DEPT together with HSQC spectroscopic data demonstrated that there are two carbonyls, ten aromatic quaternary carbons, five aromatic methines, one methene, one methoxy, and two methyls. HMBC corrections between H-1 and C-4a/C-3/C-9, H-4 and C-1a/C-2/C-10, H-7 and C-5/C-9a, and H-8

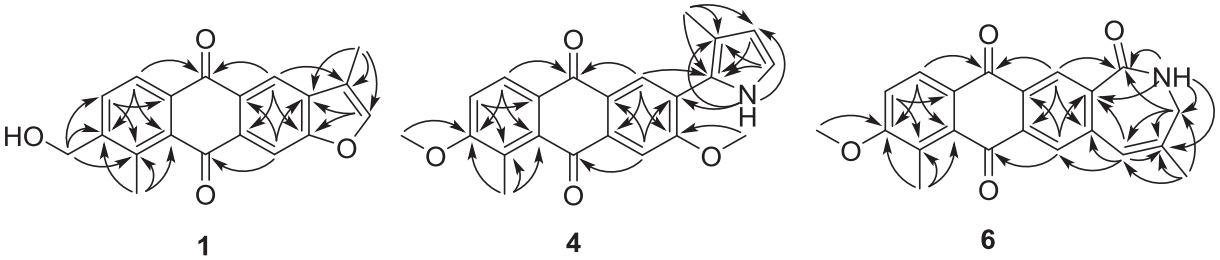

1 4 6

Fig. 2. Key HMBC correlations of compounds **1**, **4** and **6**.

and C-10a/C-6/C-9 indicated the presence of a 2,3,5,6-tetrasubstituted-9,10-anthraquinone substructure. Additionally, HMBC corrections of H-NH with C-1′/C-2/C-3′/C-4′, H_2-3′ with C-1′/C-4′/C-5′, H-5′ with C-2/C-3/C-3′/C-4′, and H_3-6′ with C-3′/C-4′/C-5′ demonstrated that there is a methyl substituted nitrogen-bearing seven-membered heterocycle as depicted in Fig. 1. Moreover, the nucleus depicted was confirmed by HMBC correlations between H-1 and C-1′, H-4 and C-5′, and H-5′ and C-4. These correlations indicated that both subunits were attached at C-2 and C-3. The remaining substituents of **6** were constructed through the HMBC correlations of H_3-7′ with C-5/C-6/C-10a, and the methoxy protons at C-6 with C-6. Ultimately, compound **6** was established as 6-methoxy-4′,5-dimethyl-2′,3′-dihydro-1′*H*-anthra[2,3-*c*]azepine-1′,9,10-trione.

Compound **7** was acquired as a reddish gum and displayed the molecular formula of $C_{21}H_{17}NO_5$, requiring 14 indices of hydrogen deficiency. The ^{1}H and ^{13}C NMR data (Table 3) are highly similar to those of **6**, with the only variation being the substitution of the methyl group at C-5 in **6** with a methoxy (δ_H 3.85; δ_C 61.2) group in **3**. The validation of these findings was established through HMBC correlations that linked the methoxy protons to C-5. Thus, compound **7** was clarified and identified as 5,6-dimethoxy-4′-methyl-2′,3′-dihydro-1′*H*-anthra[2,3-*c*]azepine-1′,9,10-trione.

3.2. Determination of inactivation, protection, and curative activities of new compounds

There is potential for anthraquinone compounds to exhibit anti-TMV activities (Ma et al., 2017; Zhou et al., 2017). New compounds were assessed for their effectiveness against TMV, and compounds **1**, **4** and **5** demonstrated obvious inactivation effects with inhibition rates of 41.6, 55.4 and 38.6% at concentrations of 50 μg/mL, respectively. These findings are reported in Table 4 and Fig. S28, and these rates are better than that of ningnanmycin (with an inhibition rate of 33.8%). The inactivation effects of compounds **6** and **7** were comparable to that of ningnanmycin, with inhibition rates of 32.5% and 34.9%, respectively. In addition, the IC_{50} values of the inactivation effects of these compounds were assessed, and the findings indicated that compounds **1**, **4**, and **5** exhibited higher efficacy than ningnamycin (Table 4).

Given that the inactivation effects of compounds **1**, **4**, and **5** were higher than those of the others, we selected these compounds for further protection activity studies. The results indicated that compounds **1**, **4** and **5** exhibited notable protective effects, with inhibition rates of 48.7% ± 4.2, 60.2% ± 3.5 and 43.5% ± 4.4, respectively (Fig. S29). These rates are better than that of ningnanmycin, which had an inhibition rate of 38.2% ± 4.6. The above results indicated that pretreatment with compounds **1**, **4** and **5** could increase the resistance of tobacco to TMV infection.

From the above results, compound **4** had the strongest inactivation effects and protective effects on TMV. To better apply the laboratory results to the actual flue-cured tobacco planting process, we selected the 5–6 leaf stage flue-cured tobacco (*N. tabacum* cv. HD, China's main flue-cured tobacco cultivar) to carry out the curative effects experiment of **4** and ningnanmycin on TMV. From the experimental results, it can be seen that the negative control group was seriously infected with TMV, the lesions were very obvious, the growth trend was slow, and the leaves were obviously deformed (Fig. 3d). This may have a serious impact on the yield and quality of tobacco leaves. However, after treatment with ningnanmycin, the lesions were significantly reduced, the disease was significantly improved, and the leaf growth tended to be normal (Fig. 3e). After treatment with **4**, the lesions were obviously further reduced compared with those after treatment with ningnanmycin. There was only a small amount of lesion observed on the newly grown leaves. The growth of tobacco plants also had a tendency to return to normal (Fig. 3f). This result shows that compound **4** has an obvious curative effect on tobacco plants infected with TMV, and its curative effect is obviously better than that of ningnanmycin. The curative effect results indicated that **4** can significantly alleviate the impact of TMV on tobacco growth and effectively improve the yield and quality of tobacco infected with TMV.

Table 4
Inactivation effects of compounds **1**–**7** on *N. glutinosa*.

Compound	Inactivation effects (%) at 50 μg/mL	IC_{50} of inactivation effects (μg/mL)
1	41.6 ± 3.2^b	55.1 ± 4.1^b
2	26.2 ± 3.0^a	98.6 ± 5.4^h
3	30.2 ± 3.2^a	85.3 ± 4.9^g
4	55.4 ± 3.4^c	40.9 ± 3.6^a
5	38.6 ± 3.6^b	63.4 ± 3.9^c
6	32.5 ± 3.3^a	79.6 ± 4.2^f
7	34.9 ± 3.1^a	68.5 ± 5.1^d
Ningnanmycin	33.8 ± 3.2^a	72.8 ± 3.5^e

Note: Different lowercase letters in the same column represent significant differences among various compounds at the 0.05 level by Duncan's multiple range test. The means ± SDs of the data obtained from three replicates are presented.

3.3. The direct action of compound *4* on TMV

Compounds **1**, **4**, and **5** demonstrated antiviral activities against TMV through inactivation, protection, and curative activity assays. Among them, **4** was found to be the most effective in controlling TMV. The inactivation effect was identified as the primary factor contributing to the antiviral activities of the compounds against TMV (Li et al., 2021). Therefore, compound **4** was selected to investigate its direct action on TMV particles and to elucidate the inactivation mechanism of these compounds on TMV through TEM. The results indicated that the TMV particles treated with compound **4** were severely fragmented, with most of them being broken into small fragments ranging from 20 to 300 nm. Additionally, the fusion phenomena caused a reduction in the number of TMV particles (Fig. 4). These findings suggest that the potent direct effect of compound **4** on TMV particles is responsible for its significant inactivation against TMV.

3.4. Effects of compounds *1*, *4* and *5* on the TMV-CP and TMV-CP genes

Systemic acquired resistance (SAR) is a desirable type of plant resistance because it has long-lasting effects and causes less damage to crops (Fujita and Inui, 2021). To investigate whether compounds **1**, **4** and **5** induced SAR and thus provided protection against TMV infection in tobacco plants, TMV-CP was analyzed using western blot assay on the host plant *N. tabacum* cv. HD. (Fig. 5)(Yan et al., 2022). As depicted in Fig. 5a, the intensity of TMV-CP bands indicated a significant decrease on the 3rd day after inoculation in the leaves treated with **1**, **4**, and **5** compared to the negative control, suggesting a reduction in the TMV-CP content. Additionally, their contents were also lower than that of ningnanmycin, and **4** had the lowest band. These results were consistent with the inhibition rates obtained from the half-leaf method. On the 7th day following inoculation, the patterns observed in the intensity of the TMV-CP bands in Fig. 5b were found to be in agreement with those seen on the 3rd day. Furthermore, the intensities of the bands for **1**, **4**, **5** and ningnanmycin were significantly lower than those on the 3rd day. This may be attributed to the induction of SAR by compounds **1**, **4**, and **5**, which inhibited virus accumulation in plants.

To further confirm the anti-TMV efficiency of compounds **1**, **4** and **5** at the transcription level, a sensitive and specific assay known as semi-quantitative RT-PCR was performed. The newly grown leaves of *N. tabacum* cv. HD on the 7th day were utilized as the sample material based on the outcomes of the western blot assay for TMV-CP. The results of the RT-PCR assay (Fig. 5c) demonstrated that *TMV-CP* expression was noticeably lower in the treatment group than in the negative control in newly grown leaves of tobacco. Furthermore, the compounds' inhibitory effects on systemic *TMV-CP* synthesis varied, with **4** exhibiting the

Fig. 3. The curative effect of compound **4** on TMV. Tobacco seedlings infected with TMV to be treated (a–c), negative control (d), treated with 100 μg/mL ningnanmycin (e) and compound **4** (f). Photos were taken 20 days after treatment.

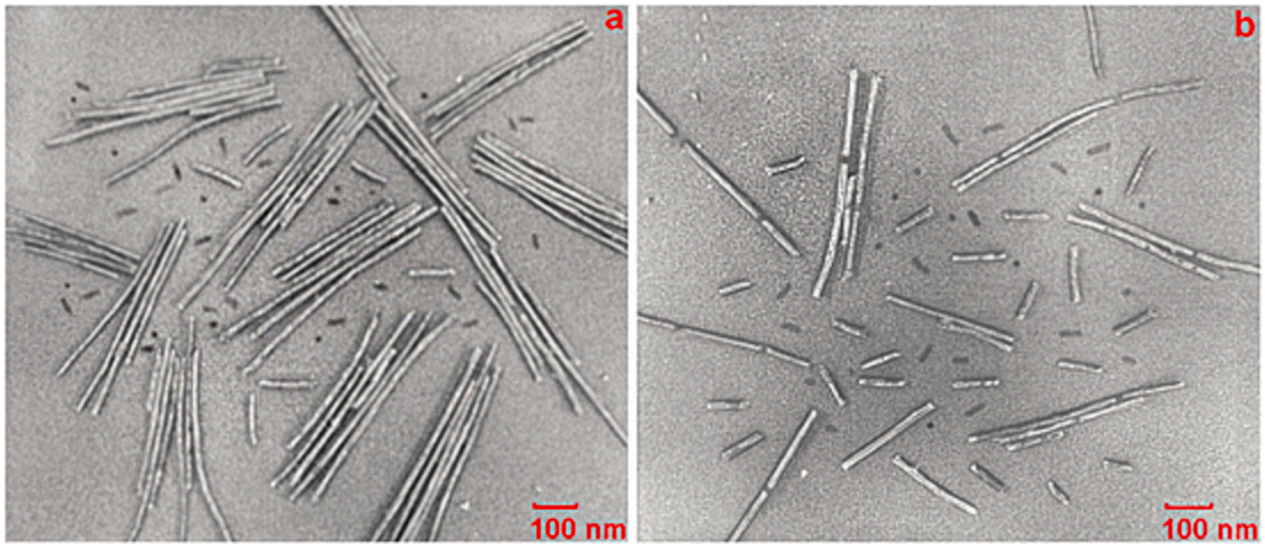

Fig. 4. TEM of TMV particles untreated (a) and treated with compound **4** (b).

highest inhibitory effect, followed by **1** and **5**, and finally ningnanmycin. These findings were consistent with those of the western blot analysis. The above observations suggested that compounds **1**, **4**, and **5** may inhibit the accumulation of the TMV-CP protein and gene, thereby exhibiting anti-TMV activities, and compound **4** indicated a relatively higher induction in systemic leaves.

3.5. *Effects of compound **4** on defense-related enzyme activities*

Since defense-related enzyme (such as PAL, POD, SOD, PPO) activities have been found to be significantly related to induced resistance in plants (Dietz et al., 2016; Fan et al., 2011), these enzyme activities were investigated in compound **4**-treated tobacco leaves. As depicted in Fig. 6, the activities of the four enzymes in the DMSO + TMV, ningnanmycin + TMV, and **4** + TMV treatment groups were considerably

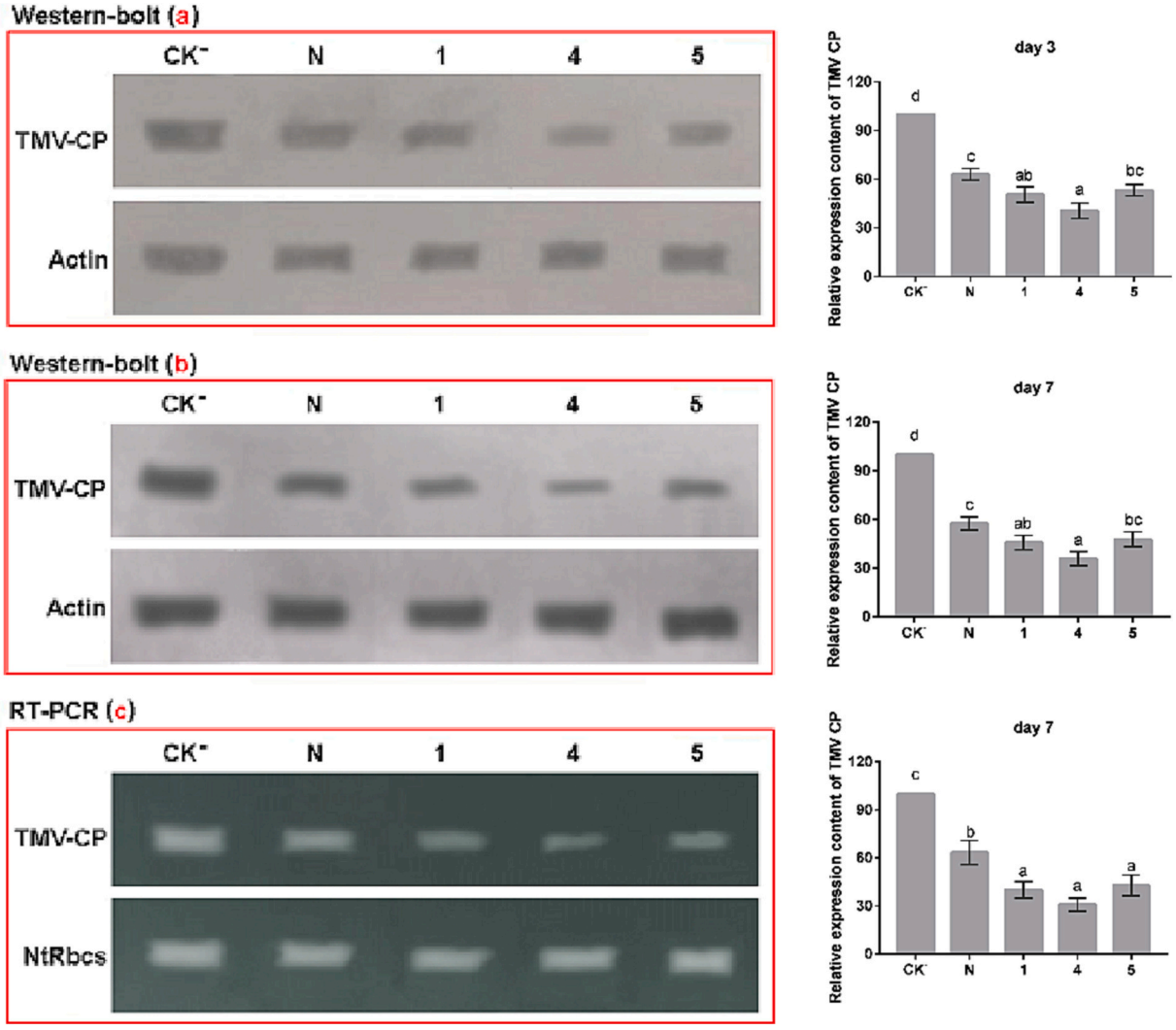

Fig. 5. Investigation of the content of TMV-CP and the *TMV-CP* gene. Western blot determination of the content of TMV-CP in the inoculated leaves with compounds **1**, **4** and **5** on the 3rd day (a) and 7th day (b). The content of *TMV-CP* in tobacco leaves on the 7th day was analyzed using RT-PCR (c). This experiment was repeated three times independently, and the outcomes were reproducible and consistent. Internal references were provided by Actin and *NtRbcs*. The negative control was denoted as CK^{-}, while ningnanmycin was denoted as N. Different lowercase letters on the column represent significant differences at the 0.05 level by Duncan's multiple range test.

greater than those in the mock group. Notably, PAL activities exhibited the greatest change. In Fig. 6a, PAL activities treated with **4** + TMV increased from the 1st day to the 5th day in tobacco leaves, peaked on the 5th day, and then declined from the 5th day to the 7th day. On the 5th day, it was discovered that the level of PAL in the **4**-treated group was 2.81-fold greater than that of the mock group, 1.85-fold greater than that of the DMSO + TMV group, and 1.59-fold greater than that of the ningnamycin + TMV group. PAL is an essential enzyme that facilitates the conversion of phenylpropanoids to cinnamic acid, ultimately leading to the production of SA, which helps in the plant's defense against pathogens (Gozzo, 2003). The group treated with **4** + TMV displayed a significant increase in POD activities compared to the mock treatment and peaked on the 3rd day (Fig. 6b). POD is an important enzyme related to plant defense that can induce the production of lignin, SA, and phytoalexins, thereby stimulating SAR and inhibiting pathogens, as well as reinforcing the cell wall (Nicholson and Hammerschmidt, 1992; Nystrom et al., 2005). From the 1st day to the 5th day, the **4** + TMV and ningnanmycin + TMV treatment groups exhibited a noticeable increase in SOD activities, with the highest level being observed on the 5th day and on the 3rd day, respectively (Fig. 6c). PPO activity increased gradually in the **4** + TMV treatment group, reaching its peak on the 3rd day. The activities were 1.37-fold greater than those of the mock group (Fig. 6d). By catalyzing the synthesis of lignin and quinone components, PPO can create a protective film that protects cells from pathogens. Moreover, PPO can produce quinones, which can play a direct role in disease resistance (Zhao et al., 2017). The defense-related enzyme activities assay conducted in this part indicated that compound **4** had the potential to enhance tobacco's disease resistance by inducing defense-related enzyme reactions.

3.6. *Effects of compound **4** on defense-related genes*

PR-1 and *PR-5* are reliable molecular markers for SAR (Anuradha et al., 2022; Mei et al., 2023; Yan et al., 2022). Therefore, we examined their expression levels in systemic leaves after treatment with compound **4**. The results are shown in Fig. 7. In the mock and DMSO + TMV groups, the gene expression of *PR-1* and *PR-5* was relatively stable. However, gene expression was significantly upregulated in the **4** + TMV and ningnanmycin + TMV groups on the 3rd day. Upregulation in the **4** + TMV group was more obvious than that in the ningnanmycin + TMV group. Additionally, the expression levels of these two genes demonstrated similar patterns in tobacco leaves that were inoculated with

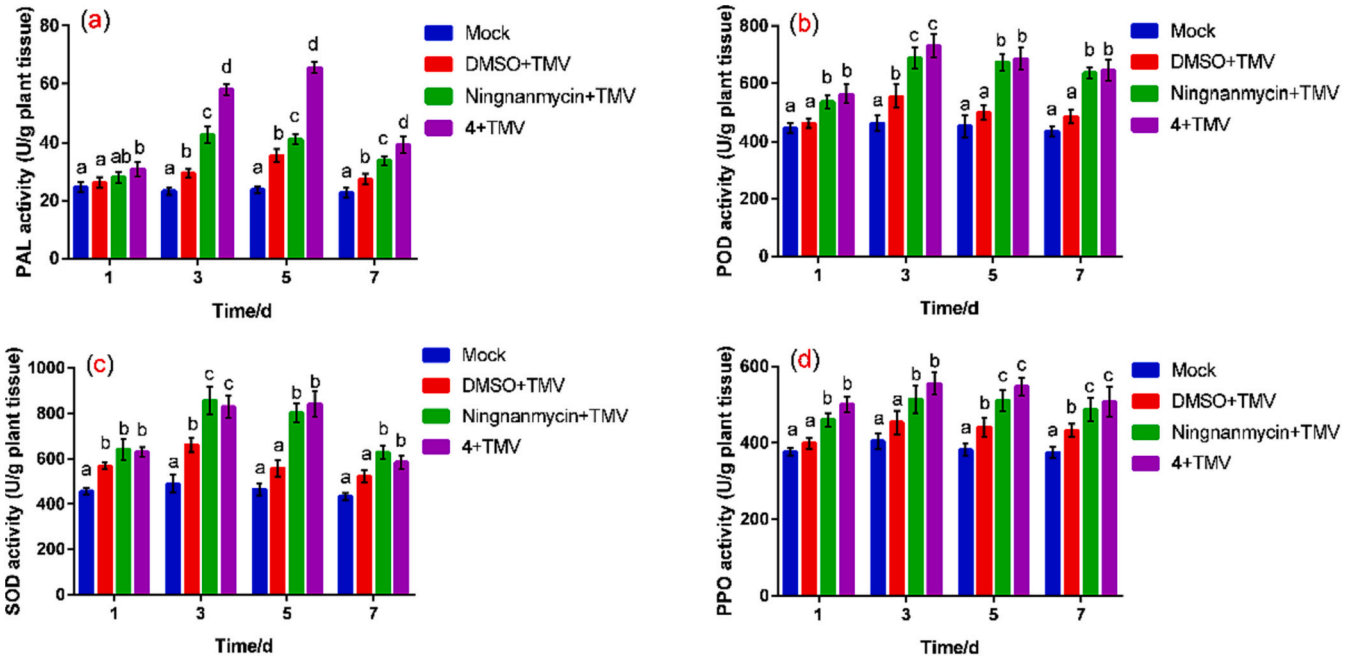

Fig. 6. The activities of PAL (a), POD (b), SOD (c), and PPO (d) were evaluated in healthy tobacco (mock), DMSO, ningnanmycin and compound **4**-treated groups. The mean ± SD values were calculated from three replicates for each group, different lowercase letters on the column represent significant differences at the 0.05 level by Duncan's multiple range test.

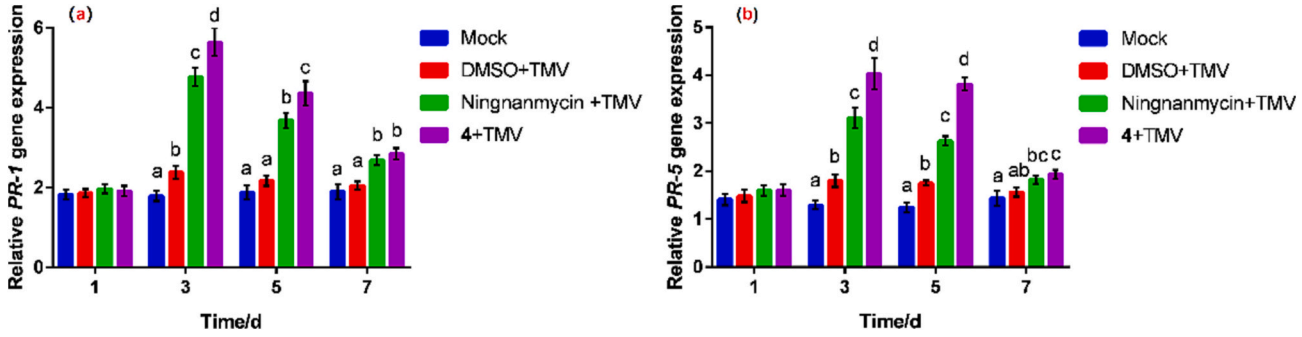

Fig. 7. Change in transcription levels of pathogenesis-related (PR) protein genes of *PR-1* (a) and *PR-5* (b). Mock, healthy tobacco. The mean ± SD values ($n = 3$) were used to present the data. Different lowercase letters in the column represent significant differences at the 0.05 level by Duncan's multiple range test.

pathogens and peaked on Day 3 and then gradually declined. These findings suggested that compound **4** can enhance tobacco plant disease resistance by upregulating the expression of defense-related genes.

3.7. *Effects of compound **4** on SA content*

PAL is responsible for the production of SA for defense against pathogens, and SA is a natural plant defense hormone that is a key signaling molecule that activates SAR by regulating the increased

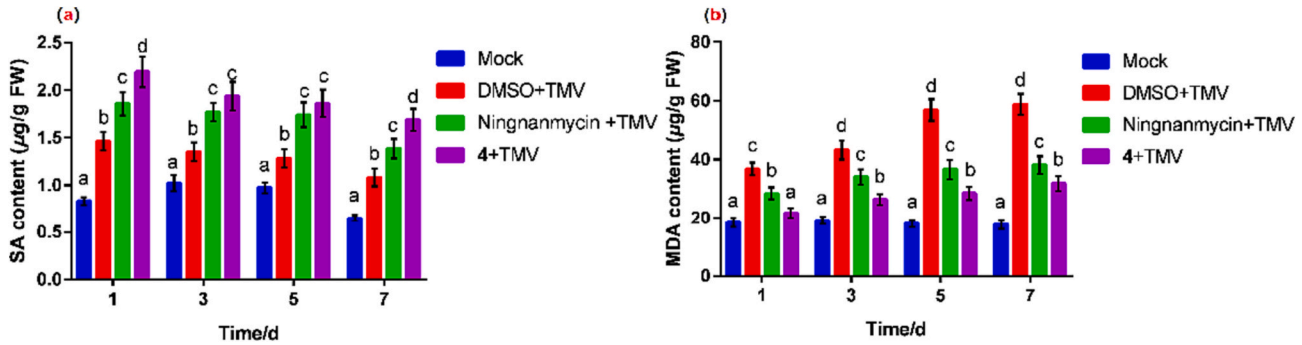

Fig. 8. Effects of compound **4** on SA (a) and MDA (b) content. Mock, healthy tobacco. Values are means ± SDs (n = 3). Different lowercase letters in the column represent significant differences at the 0.05 level by Duncan's multiple range test.

expression of several PR genes. An increase in SA levels in the plant is typically associated with SAR (Jiang et al., 2022; Peng et al., 2021). Thus, the SA content was examined in tobacco plants treated with compound **4**. The results suggested that the content of SA in tobacco plants declined gradually with TMV inoculation. In the **4** + TMV treatment group, the SA content peaked on the 1st day and gradually decreased from the 3rd to the 7th day. The trend variation of the **4** + TMV treatment group was superior to that of the ningnanmycin + TMV treatment group (Fig. 8a). Thus, compound **4** may increase the content of SA and enhance plant resistance to disease.

3.8. Effects of compound *4* on MDA content

Malondialdehyde (MDA) is a physiological indicator that indicates the degree of cell membrane damage and lipid peroxidation, and it is often used to reflect the strength of plant responses to stress conditions (Kwiecien et al., 2014; Zhang et al., 2020). When using disease-resistant substances to treat infected plants, it can inhibit the increase in MDA content in plants, thus exerting protective effects (Khalil et al., 2021). In this study, analysis of the MDA levels in tobacco leaves was conducted after treatment with compound **4**. As displayed in Fig. 8b, the MDA content in mock was not obvious and remained at a low level. However, in the DMSO + TMV group, there was a notable rise in the MDA content. Compared with the DMSO + TMV group, after treatment with compound **4**, there was a notable reduction in the MDA content, which was better than that of the ningnanmycin + TMV group. These results indicated that compound **4** could effectively reduce the MDA content in tobacco leaves, thereby reducing the extent of plant damage caused by TMV infection.

3.9. Effects of compounds on total protein Hsp70 expression and transcription levels of Hsp70 genes

The plant Hsp70 protein shares similarities with its animal counterpart in terms of its response to stress (Wang et al., 2004). In TMV-infected plants, the expression of Hsp70 can be triggered. This, in turn, facilitates the accumulation and movement of the virus within the plants (Yan et al., 2022). Therefore, the expression of total NtHsp70 protein in tobacco leaves on the 7th day was investigated by western blot. The results indicated that the expression of total NtHsp70 protein in the CK^- and compounds **1**-, **4**- and **5**-treated groups was higher than that in the healthy tobacco group (mock). However, the total NtHsp70 expression levels of compounds **1**, **4** and **5** treatment groups were decreased compared with the CK^- group, and the expression levels of the **4** group were the lowest (Fig. 9a).

Furthermore, in recently published literature (Wang et al., 2022; Yan et al., 2022), the downregulated expression of the *NbHsp70cp-1*, *NbHsp70c-A*, *NtHsp70–1*, and *NtHsp70–261* genes is closely related to the anti-TMV activities of natural compounds. Thus, we synthesized four pairs of specific primers for these genes (Table S1) and conducted qRT-PCR analysis (Fig. 9b). The results revealed that while the expression levels of the four genes were upregulated in tobacco leaves inoculated with TMV, they were significantly downregulated in the compound **4** treatment group. Thus, the proliferation of TMV may be inhibited by downregulation of the expression of NtHsp70 protein and some of the important Hsp70 genes, thereby achieving control of TMV.

3.10. Molecular docking of new compounds

To further understand the structure-activity relationship of compounds **1**–**7**, the molecular docking was conducted. The molecular weight of the protein is 27.63 kDa and it comprises 159 amino acids. The protein crystal structure shows that this protein is a polymer, in which the 5-mer can encapsulate a pocket, and the active pocket of the protein consists of Thr42-Arg46-Gln45-Arg90-Arg92, Asn33-Gln34-Gln39-Ala40-Gln38-Thr37, Asn127-Ser123-Val119-Asp116, forming a more hydrophilic pocket (Fig. 10). Compound **1** forms hydrogen bonds with Asn127 and Arg90 in the docking model, while compounds **2** and **3** lose hydrogen bonds with Asn127, so the activity of **1** is stronger than those of **2** and **3**. The hydroxyl group in compound **3** may form a water bridge with the protein, leading to a weaker activity for **2** compared to **3**. Compound **4** has one more five-membered ring, which can occupy more space to form more hydrophobic interactions, so the activity of **4** is improved. Compound **5** can only form a hydrogen bond with protein, resulting in weaker activity than **1**. Compounds **6** and **7** have atomic conflicts with protein, so the activity is weaker than that of **4**. The preceding outcomes of molecular docking corroborated the previous anti-TMV efficacy. Meanwhile, it was further indicated that compound **4** had the strongest activity.

The above molecular docking results revealed that the anthraquinone nucleus can interact with TMV-CP proteins, which may be fundamental for its direct effect on TMV and disease resistance. In addition, the 3′-methyl-1′*H*-pyrrol-2′-yl moiety substituted on anthraquinone or the hydroxyl and methoxy groups can notably increase the activity against TMV. This structure-activity relationship is proposed by our work in natural products for the first time and is helpful for finding new anti-TMV inhibitors.

3.11. Antirotavirus activities of new compounds

To investigate whether anthraquinones have a broad spectrum of potential antiviral effects, compounds **1**–**7** were also subjected to

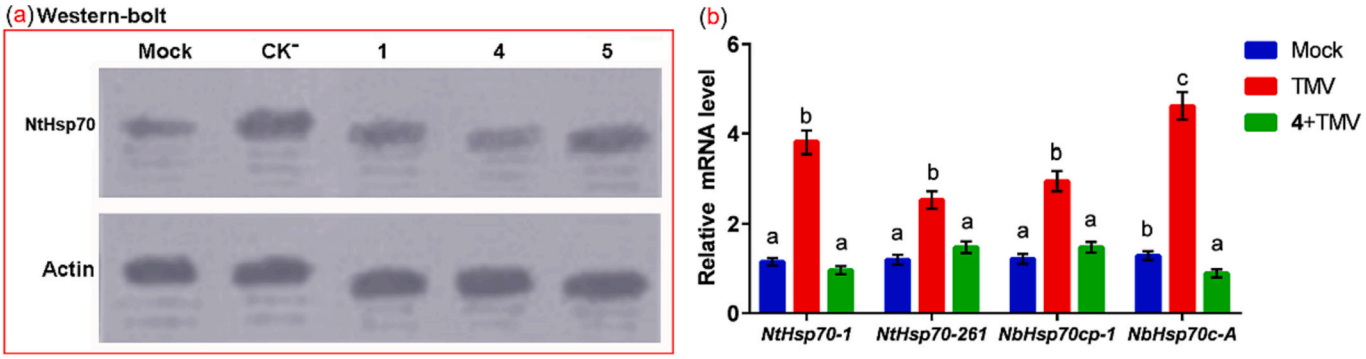

Fig. 9. Investigation of the expression levels of total NtHsp70 protein together with *Hsp70* genes. (a) Investigation of the expression of NtHsp70 by western blot in the inoculated leaves on the 7th day after treatment with compounds **1**, **4** and **5**. Similar outcomes were acquired from three separate assays. (b) On the 7th day, the accumulation of *NtHsp70–1*, *NtHsp70–261*, *NbHsp70cp-1*, and *NbHsp70c-A* was assessed in the bottom leaves with **4** treatments using qRT-PCR. The negative control was denoted as CK^- and healthy tobacco was denoted as the mock. Actin was utilized as the internal reference. Different lowercase letters in the column represent significant differences at the 0.05 level by Duncan's multiple range test.

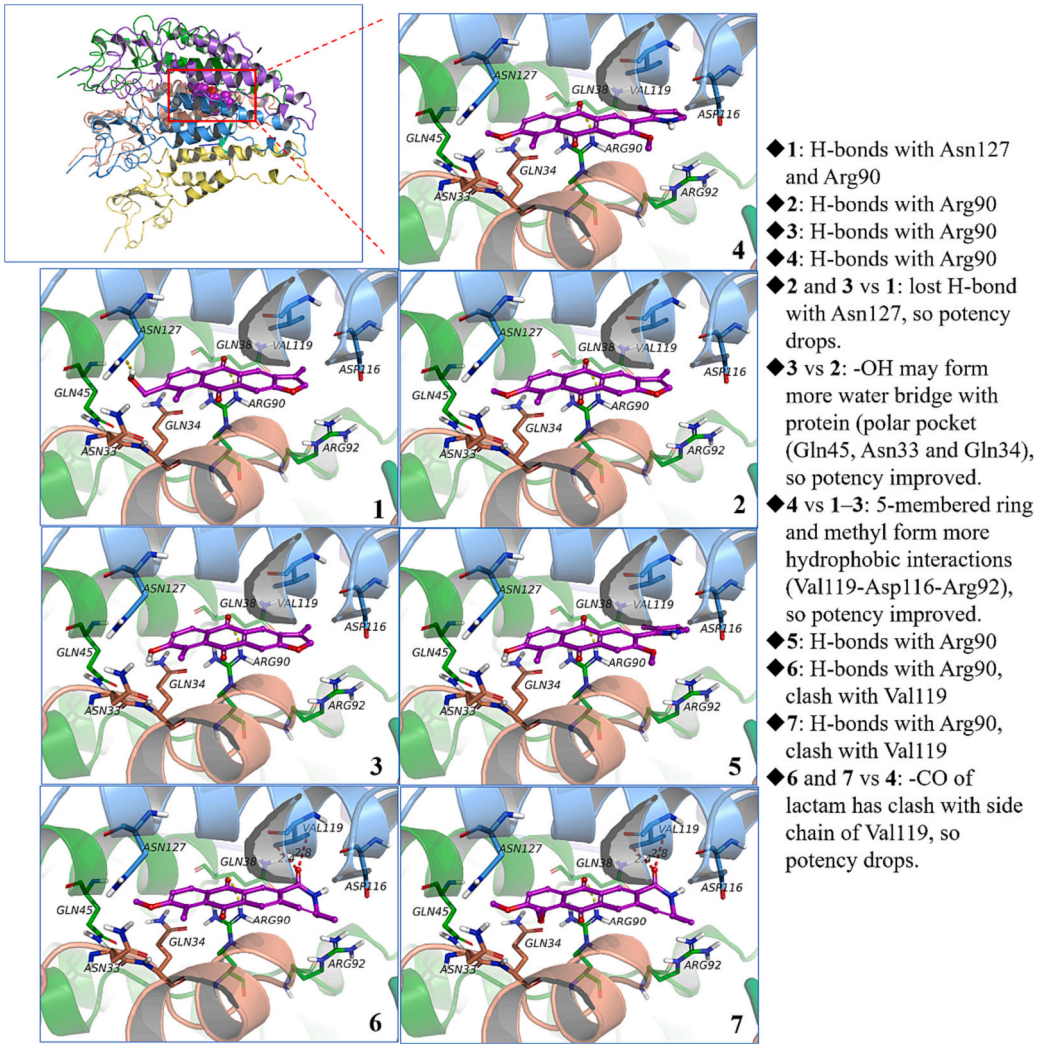

Fig. 10. Interactions between TMV-helicase (sticks are used to represent key residues while solid lines indicate H-bonds) and compounds **1**–**7**.

antirotavirus assays. In line with our previous research (Hu et al., 2021), we assessed their ability to inhibit rotavirus-induced cytopathic effects in MA104 cells and used ribavirin as a positive control agent to ensure the validity of the results. The results (shown in Table 5) indicated that isolates **1**–**7** possess robust antirotavirus activities, with TI values ranging from 11.6 to 17.7. It should be noted that these values were slightly lower than that of the positive control agent (22.9).

4. Conclusion

As a result, seven new rare derivatives of anthraquinones (**1**–**7**) were obtained. Apart from compounds **4** and **5**, the nuclei of the remaining new compounds were discovered for the first time in nature. Among them, **1**–**3** bear an unusual anthra[2,3-*b*]furan-9,10-dione nucleus, **4** and **5** possess a rare 3-methyl-1*H*-pyrrol-2-yl substituent, and surprisingly, **6** and **7** are the new framework anthraquinones bearing a 6-methyl-1,7-dihydro-2*H*-azepin-2-one ring. Tested compounds **1**, **4**, and **5** exhibited better protective effects against TMV than the commercially available anti-TMV agent, ningnanmycin. These compounds have the ability to reduce the amount of TMV-CP protein and gene expression, especially compound **4**, which had the best protective effect. Compound **4** was found to act on TMV particles through a combination of fracture or distortion of virus particles into small fragments and fusion phenomena, and the breakdown of TMV particles by **4** was largely attributed to its interaction with the TMV-CP protein. Compound **4** was found to significantly boost the defense enzyme activities, raise the content of SA, reduce the content of MAD, and stimulate the upregulation of disease-resistance genes in tobacco leaves that were infected with TMV. This suggests that compound **4** possesses the potential to induce resistance and increase the tolerance of plants to TMV infection. Additionally, compound **4** was found to decrease the overall amount of NtHsp70 protein and downregulate the expression of *Hsp70* genes in TMV-infected tobacco. To the best of our knowledge, this is the first study to prove that these anthraquinones, especially **4**, have the potential to be used as inducers of plant SAR and as new plant protective agents that can induce inherent disease resistance mechanisms in plants. It was also

Table 5
The activities of compounds **1**–**7** against rotavirus.

Compound	CC_{50} (μg/mL)	EC_{50} (μg/mL)	TI (CC_{50}/EC_{50})
1	225.4	13.0	17.3
2	176.2	12.6	14.0
3	185.0	15.9	11.6
4	268.9	15.2	17.7
5	232.6	18.8	12.4
6	224.3	14.4	15.6
7	242.1	15.5	15.6
Ribavirin	284.5	12.4	22.9

The CC_{50} represents the half cytotoxic concentration, while the EC_{50} represents the half effective concentration. The therapeutic index (TI) can be calculated as CC_{50} divided by EC_{50}.

found that **4** could downregulate the expression of *Hsp70* genes, suggesting that the expression of *Hsp70* genes may be suppressed by these compounds, potentially leading to the inhibition of TMV spread. **4** can directly act on TMV particles, causing them to breakdown, thereby achieving an anti-TMV effect. These anthraquinones have different mechanisms of action to achieve resistance to TMV virus.

Apart from their anti-TMV properties, isolates **1**–**7** demonstrated promising antirotavirus activities, with a TI range of 11.6–17.7, which was slightly lower than that of the positive control (TI = 22.9). The successful purification and identification of anthraquinone isolates, together with comprehensive research on their anti-TMV mechanism and antirotavirus activities, have provided valuable resources for the identification of antiviral inhibitors, particularly those targeting TMV. Additionally, these findings have made significant contributions to the development and exploration of microorganisms derived from tobacco.

CRediT authorship contribution statement

Feng-Xian Yang: Data curation, Methodology, Writing – review & editing. **Yue-Yu Ma:** Data curation. **Yu-Ping Wu:** Methodology. **Gao-Kun Zhao:** Validation. **Yong-Ping Li:** Validation. **Zhen-Jie Li:** Validation. **Xue-Mei Li:** Formal analysis. **Yin-Ke Li:** Investigation. **Wei-Guang Wang:** Investigation. **Min Zhou:** Investigation. **Guang-Hui Kong:** Conceptualization, Project administration, Funding acquisition, Supervision. **Qiu-Fen Hu:** Conceptualization, Project administration, Funding acquisition, Supervision.

Declaration of Competing Interest

The authors declare that no competing interests exist.

Data availability

Data will be made available on request.

Acknowledgments

The National Natural Science Foundation of China (No. 21967021) provided financial support for this project, as did the Yunnan Tobacco Company Foundation (No. 2020530000241001 and 2021530000241002) and the Yunnan Innovative Research Team Foundation (2019HC020).

Appendix A. Supplementary data

Supplementary data to this article can be found online at https://doi.org/10.1016/j.pestbp.2023.105613.

References

Akhter, N., Pan, C., Liu, Y., Shi, Y., Wu, B., 2019. Isolation and structure determination of a new indene derivative from endophytic fungus *Aspergillus flavipes* Y-62. Nat. Prod. Res. 33 (20), 2939–2944. https://doi.org/10.1080/14786419.2018.1510399.

Anuradha, C., Chandrasekar, A., Backiyarani, S., Thangavelu, R., Giribabu, P., Uma, S., 2022. Genome-wide analysis of pathogenesis-related protein 1 (PR-1) gene family from *Musa* spp. and its role in defense response during stresses. Gene 821, 146334. https://doi.org/10.1016/j.gene.2022.146334.

Das, J.K., Bhutta, Z.A., 2016. Global challenges in acute diarrhea. Curr. Opin. Gastroenterol. 32 (1), 18–23. https://doi.org/10.1097/MOG.0000000000000236.

Dietz, K.J., Turkan, I., Krieger-Liszkay, A., 2016. Redox-and reactive oxygen species-dependent signaling into and out of the photosynthesizing chloroplast. Plant Physiol. 171 (3), 1541–1550. https://doi.org/10.1104/pp.16.00375.

Dufossé, L., 2014. Anthraquinones, the Dr Jekyll and Mr Hyde of the food pigment family. Food Res. Int. 65, 132–136. https://doi.org/10.1016/j.foodres.2014.09.012.

Fan, H.T., Song, B.A., Bhadury, P.S., Jin, L.H., Hu, D.Y., Yang, S., 2011. Antiviral activity and mechanism of action of novel thiourea containing chiral phosphonate on tobacco mosaic virus. Int. J. Mol. Sci. 12 (7), 4522–4535. https://doi.org/10.3390/ijms12074522.

Fujita, K., Inui, H., 2021. Review: biological functions of major latex-like proteins in plants. Plant Sci. 306, 110856 https://doi.org/10.1016/j.plantsci.2021.110856.

Ge, H.M., Song, Y.C., Shan, C.Y., Ye, Y.H., Tan, R.X., 2005. New and cytotoxic anthraquinones from *Pleospora* sp. IFB-E006, an endophytic fungus in *Imperata cylindrical*. Planta Med. 71 (11), 1063–1065. https://doi.org/10.1055/s-2005-864190.

Gombodorj, S., Yang, M.H., Shang, Z.C., Liu, R.H., Li, T.X., Yin, G.P., Kong, L.Y., 2017. New phenalenone derivatives from *Pinellia ternata* tubers derived *Aspergillus* sp. Fitoterapia 120, 72–78. https://doi.org/10.1016/j.fitote.2017.05.014.

Gooding Jr., G.V., Hebert, T.T., 1967. A simple technique for purification of tobacco mosaic virus in large quantities. Phytopathology 57 (11), 1285. https://doi.org/10.1098/rstl.1767.0047.

Gozzo, F., 2003. Systemic acquired resistance in crop protection: from nature to a chemical approach. J. Agric. Food Chem. 51 (16), 4487–4503. https://doi.org/10.1021/jf030025s.

Hagag, A., Abdelwahab, M.F., Abd El-Kader, A.M., Fouad, M.A., 2022. The endophytic *Aspergillus* strains: a bountiful source of natural products. J. Appl. Microbiol. 132 (6), 4150–4169. https://doi.org/10.1111/jam.15489.

Hosoe, T., Nozawa, K., Udagawa, S., Nakajima, S., Kawai, K., 1990. An anthraquinone derivative from *Dichotomophthora lutea*. Phytochemistry 29 (3), 997–999. https://doi.org/10.1016/0031-9422(90)80068-R.

Hu, Q.F., Zhou, B., Huang, J.M., Gao, X.M., Shu, L.D., Yang, G.Y., Che, C.T., 2013. Antiviral phenolic compounds from *Arundina gramnifolia*. J. Nat. Prod. 76 (2), 292–296. https://doi.org/10.1021/np300727f.

Hu, Q.F., Wu, F., Zhou, T., Zhou, M., Zhu, Y.N., Cai, B.B., Liu, M.X., Li, M.F., Yang, G.Y., Li, Y.K., 2021. Three new anti-rotavirus chromeno [3, 2-c] pyridines from the whole plant of *Thalictrum scabrifolium*. Heterocycles 102 (9), 1810–1816. https://doi.org/10.3987/com-21-14505.

Hu, Z., Bo, X., Sun, G., Zhao, L., Shi, C., Huang, L., Tian, X., 2022. Identification of vanillic acid and its new amide derivative from *Hyoscyamus niger* and their modes of action in controlling tobacco mosaic virus. Ind. Crop. Prod. 189, 115853 https://doi.org/10.1016/j.indcrop.2022.115853.

Ibrahim, S.R.M., Elkhayat, E.S., Mohamed, G.A., Khedr, A.I.M., Fouad, M.A., Kotb, M.H.R., Ross, S.A., 2015. Aspernolides F and G, new butyrolactones from the endophytic fungus *Aspergillus terreus*. Phytochem. Lett. 14, 84–90. https://doi.org/10.1016/j.phytol.2015.09.006.

Jiang, Y., Ji, X., Zhang, Y., Pan, X., Yang, Y., Li, Y., Guo, W., Wang, Y., Ma, Z., Lei, B., Yan, H., Liu, X., 2022. Citral induces plant systemic acquired resistance against tobacco mosaic virus and plant fungal diseases. Ind. Crop. Prod. 183, 114948 https://doi.org/10.1016/j.indcrop.2022.114948.

Khalil, M.I.I., Youssef, S.A., Tartoura, K.A., Eldesoky, A.A., 2021. Comparative evaluation of physiological and biochemical alteration in tomato plants infected by *Alternaria alternata* in response to *Trichoderma viride* and *Chaetomium globosum* application. Physiol. Mol. Plant P. 115, 101671. https://doi.org/10.1016/j.pmpp.2021.101671.

Kwiecien, S., Jasnos, K., Magierowski, M., Sliwowski, Z., Pajdo, R., Brzozowski, B., Mach, T., Wojcik, D., Brzozowski, T., 2014. Lipid peroxidation, reactive oxygen species and antioxidative factors in the pathogenesis of gastric mucosal lesions and mechanism of protection against oxidative stress-induced gastric injury. J. Physiol. Pharmacol. 65 (5), 613–622 (PMID: 25371520).

Li, Y., Ye, S., Hu, Z., Hao, N., Bo, X., Liang, H., Tian, X., 2021. Identification of anti-TMV active flavonoid glycosides and their mode of action on virus particles from *Clematis lasiandra* maxim. Pest Manag. Sci. 77 (11), 5268–5277. https://doi.org/10.1002/ps.6569.

Liang, Z., Zhang, T., Zhang, X., Zhang, J., Zhao, C., 2015. An alkaloid and a steroid from the endophytic fungus *Aspergillus fumigatus*. Molecules 20 (1), 1424–1433. https://doi.org/10.3390/molecules20011424.

Lim, F.Y., Hou, Y., Chen, Y., Oh, J.H., Lee, I., Bugni, T.S., Keller, N.P., 2012. Genome-based cluster deletion reveals an endocrocin biosynthetic pathway in *Aspergillus fumigatus*. Appl. Environ. Microbiol. 78 (12), 4117–4125. https://doi.org/10.1128/AEM.07710-11.

Liu, Z., Zhao, J.Y., Sun, S.F., Li, Y., Qu, J., Liu, H.T., Liu, Y.B., 2019. Sesquiterpenes from an endophytic *Aspergillus flavus*. J. Nat. Prod. 82 (5), 1063–1071. https://doi.org/10.1021/acs.jnatprod.8b01084.

Ma, T.T., Shan, W.G., Ying, Y.M., Ma, L.F., Liu, W.H., Zhan, Z.J., 2015. Xanthones with α-glucosidase inhibitory activities from *Aspergillus versicolor*, a fungal endophyte of *Huperzia serrata*. Helv. Chim. Acta 98 (1), 148–152. https://doi.org/10.1002/hlca.201400165.

Ma, H.Y., Liu, L.X., Yang, G.R., Liu, Q., Yang, Y., Zhou, L., Xing, H.H., Zhou, M., Ye, Y.Q., Wu, H.Y., Du, G., Li, X.M., Hu, Q.F., 2017. Anthraquinones from the barks of *Cassia alata* and their anti-tobacco mosaic virus activity. Chem. Nat. Compd. 53 (5), 852–855. https://doi.org/10.1007/s10600-017-2139-4.

Malla, B.A., Rafiq, S., Hadi, A., Ali, A., Kaloo, Z.A., Wagay, N.A., Dar, N.H., 2023. Downregulation of pro-inflammatory markers NF-κB1, RelA and COX-2 using *Aconitum chasmanthum* Stapf ex Holmes-in vitro and in-silico study. Ind. Crop. Prod. 197, 116564 https://doi.org/10.1016/j.indcrop.2023.116564.

Masi, M., Evidente, A., 2020. Fungal bioactive anthraquinones and analogues. Toxins (Basel) 12 (11), 714. https://doi.org/10.3390/toxins12110714.

Mei, J., Guo, D., Wang, J., Wang, S., 2023. Characterization of rice and maize constitutive expresser of pathogenesis-related genes 5 in plant immunity. Eur. J. Plant Pathol. 165, 203–212. https://doi.org/10.1007/s10658-022-02584-w.

Mi, K., Ou, X., Guo, L., Ye, J., Wu, J., Yi, S., Niu, X., Sun, X., Li, H., Sun, M., 2017. Comparative analysis of the immunogenicity of monovalent and multivalent rotavirus immunogens. PLoS One 12 (2), e0172156. https://doi.org/10.1371/journal.pone.0172156.

Nicaise, V., 2014. Crop immunity against viruses: outcomes and future challenges. Front. Plant Sci. 5, 660. https://doi.org/10.3389/fpls.2014.00660.

Nicholson, R.L., Hammerschmidt, R.E., 1992. Phenolic compounds and their role in disease resistance. Annu. Rev. Phytopathol. 30, 369–389. https://doi.org/10.1146/annurev.py.30.090192.002101.

Nystrom, L., Makinen, M., Lampi, A.M., Piironen, V., 2005. Antioxidant activity of steryl ferulate extract from rye and wheat bran. J. Agric. Food Chem. 53 (7), 2503–2510. https://doi.org/10.1021/jf048051t.

Olaoluwa, O.O., Aiyelaagbe, O.O., Irwin, D., Reid, M., 2013. Novel anthraquinone derivatives from the aerial parts of *Antigonon leptopus* Hook & Arn. Tetrahedron 69 (33), 6906–6910. https://doi.org/10.1016/j.tet.2013.05.014.

Peng, Y., Yang, J., Li, X., Zhang, Y., 2021. Salicylic acid: biosynthesis and signalin. Annu. Rev. Plant Biol. 72, 761–791. https://doi.org/10.1146/annurev-arplant-081320-092855.

Qin, J., Lyu, A., Zhang, Q.H., Yang, L., Zhang, J., Wu, M.D., Li, G.Q., 2019. Strain identification and metabolites isolation of *Aspergillus capensis* CanS-34A from *Brassica napus*. Mol. Biol. Rep. 46 (3), 3451–3460. https://doi.org/10.1007/s11033-019-04808-5.

Sachse, C., Chen, J.Z., Coureux, P.D., Stroupe, M.E., Fandrich, M., Grigorieff, N., 2007. High-resolution electron microscopy of helical specimens: a fresh look at tobacco mosaic virus. J. Mol. Biol. 371 (3), 812–835. https://doi.org/10.1016/j.jmb.2007.05.088.

Sadorn, K., Saepua, S., Boonyuen, N., Laksanacharoen, P., Rachtawee, P., Prabpai, S., Kongsaeree, P., Pittayakhajonwut, P., 2016. Allahabadolactones A and B from the endophytic fungus, *Aspergillus allahabadii* BCC45335. Tetrahedron 72 (4), 489–495. https://doi.org/10.1016/j.tet.2015.11.056.

Song, B., Yang, S., Jin, L.H., Bhadury, P.S., 2011. Environment-Friendly Antiviral Agents for Plants. Springer Science & Business Media.

Sun, Y., Gong, X., Tan, J.Y., Kang, L., Li, D., Vikash, Yang J., Du, G., 2016. In vitro antiviral activity of *Rubia cordifolia* aerial part extract against rotavirus. Front. Pharmacol. 7, 308. https://doi.org/10.3389/fphar.2016.00308.

Tawfike, A.F., Romli, M., Clements, C., Abbott, G., Young, L., Schumacher, M., Diederich, M., Farag, M., Edrada-Ebel, R., 2019. Isolation of anticancer and anti-trypanosome secondary metabolites from the endophytic fungus *Aspergillus flocculus* via bioactivity guided isolation and MS based metabolomics. J. Chromatogr. B Anal. Technol. Biomed. Life Sci. 1106-1107, 71–83. https://doi.org/10.1016/j.jchromb.2018.12.032.

Tikhomirov, A.S., Shchekotikhin, A.E., Luzikov, Y.N., Korolev, A.M., Preobrazhenskaya, M.N., 2014. Pd-catalyzed cross-coupling/heterocyclization domino reaction: facile access to anthra[2,3-*b*] furan-5,10-dione scaffold. Tetrahedron 70 (43), 8062–8066. https://doi.org/10.1016/j.tet.2014.08.033.

Wang, W., Vinocur, B., Shoseyov, O., Altman, A., 2004. Role of plant heat-shock proteins and molecular chaperones in the abiotic stress response. Trends Plant Sci. 9 (5), 244–252. https://doi.org/10.1016/j.tplants.2004.03.006.

Wang, J., Hao, K., Yu, F., Shen, L., Wang, F., Yang, J., Su, C., 2022. Field application of nanoliposomes delivered quercetin by inhibiting specific hsp70 gene expression against plant virus disease. J. Nanobiotechnol. 20 (1), 16. https://doi.org/10.1186/s12951-021-01223-6.

Wu, F., Zhu, Y.N., Hou, Y.T., Mi, Q.L., Chen, J.H., Zhang, C.M., Miao, D., Zhou, M., Wang, W.G., Hu, Q.F., Ye, Y.Q., Li, X.M., 2021. Two new antibacterial anthraquinones from cultures of an endophytic fungus *Phomopsis* sp. Chem. Nat. Compd. 57, 823–827. https://doi.org/10.1007/s10600-021-03489-6.

Xiao, J.J., Liao, M., Chu, M.J., Ren, Z.L., Zhang, X., Lv, X.H., Cao, H.Q., 2015. Design, synthesis, and anti-tobacco mosaic virus (TMV) activity of 5-chloro-N-(4-cyano-1-aryl-1H-pyrazol-5-yl)-1-aryl-3-methyl-1H-pyrazole-4-carboxamide derivatives. Molecules 20 (1), 807–821. https://doi.org/10.3390/molecules20010807.

Yan, W., Wuringege, Li S.J., Guo, Z.K., Zhang, W.J., Wei, W., Tan, R.X., Jiao, R.H., 2017. New *p*-terphenyls from the endophytic fungus *Aspergillus* sp. YXf3. Bioorg. Med. Chem. Lett. 27 (1), 51–54. https://doi.org/10.1016/j.bmcl.2016.11.033.

Yan, Y., Tang, L., Hu, J.Q., Wang, J.T., Adelakun, T.A., Yang, D.Q., Di, Y.T., Zhang, Y., Hao, X.J., 2018. Munronin O, a potential activator for plant resistance. Pestic. Biochem. Physiol. 146, 13–18. https://doi.org/10.1016/j.pestbp.2018.02.001.

Yan, Y., Wang, D., Zhang, X., Peng, M., Yan, X., Guo, Y., Jia, M., Zhou, J., Tang, L., Hao, X., 2022. Anti-TMV activity and effects of three prieurianin-type limonoids from *Munronia henryi*. Pestic. Biochem. Physiol. 184, 105108 https://doi.org/10.1016/j.pestbp.2022.105108.

Yang, F.X., Dai, J.M., Liu, H.Y., Mi, Q.L., Wang, J., Zhang, J.D., Li, X.M., Wang, W.G., Zhou, M., Li, Y.K., Hu, Q.F., 2022a. Isochromenes from the *Nicotiana tabacum*-derived endophytic fungus *Aspergillus versicolor* and their anti-tobacco mosaic virus activities. Nat. Prod. Res. 37 (10), 1608–1616. https://doi.org/10.1080/14786419.2022.2103554.

Yang, G.Y., Dai, J.M., Mi, Q.L., Li, Z.J., Li, X.M., Zhang, J.D., Wang, J., Li, Y.K., Wang, W.G., Zhou, M., Hu, Q.F., 2022b. Cyclopiazonic acid type indole alkaloids from *Nicotiana tabacum*-derived fungus *Aspergillus versicolor* and their anti-tobacco mosaic virus activities. Phytochemistry 198, 113137. https://doi.org/10.1016/j.phytochem.2022.113137.

Zhang, K., Yu, M., Xu, P., Zhang, S., Benoit, G., 2020. Physiological and morphological response of *Aphanizomenon flos-aquae* to watermelon (*Citrullus lanatus*) peel aqueous extract. Aquat. Toxicol. 225, 105548 https://doi.org/10.1016/j.aquatox.2020.105548.

Zhao, L.H., Dong, J.H., Zhong, H.H., Li, S.L., Su, X.X., Zhang, J., Yin, Y.Y., Xu, T., Zhang, Z.K., Chen, H.R., 2017. Anti-TMV activity and functional mechanism of two sesquiterpenoids isolated from *Tithonia diversifolia*. Pestic. Biochem. Physiol. 140, 24–29. https://doi.org/10.1016/j.pestbp.2017.05.009.

Zhou, M., Zhou, K., Gao, X.M., Jiang, Z.Y., Lv, J.J., Liu, Z.H., Yang, G.Y., Miao, M.M., Che, C.T., Hu, Q.F., 2015. Fistulains A and B, new bischromones from the bark of *Cassia fistula*, and their activities. Org. Lett. 17 (11), 2638–2641. https://doi.org/10.1021/acs.orglett.5b01007.

Zhou, M., Xing, H.H., Yang, Y., Wang, Y.D., Zhou, K., Dong, W., Li, G.P., Hu, W.Y., Liu, Q., Li, X.M., Hu, Q.F., 2017. Three new anthraquinones from the twigs of *Cassia fistula* and their bioactivities. J. Asian Nat. Prod. Res. 19 (11), 1073–1078. https://doi.org/10.1080/10286020.2017.1285911.